RESEARCH

An electric kickscooter multibody model: equations of motion and linear stability analysis

A.G. Agúndez¹ · D. García-Vallejo¹ · E. Freire²

© The Author(s) 2024

Abstract
In this work, a detailed multibody model of an electric kickscooter is presented. The model includes toroidal wheels as well as rear and front suspensions. The equations of motion are derived and linearized along the steady forward motion of the vehicle. Using an efficient linearization approach, suitable for complex multibody systems with holonomic and nonholonomic constraints, allows for obtaining the reduced linearized equations of motion as a function of the geometric, dynamic, wheels', and suspensions' parameters. The proposed electric kickscooter multibody model is validated with the stability results of a previously presented electric kickscooter benchmark. Since the resulting eigenvalues are parameterized regarding the design parameters, a detailed linear stability analysis of the system is performed. In particular, the influence on the stability of the toroidal geometry of the wheels, the elliptic cross-section of the toroidal wheels, the rider model, the steering axis inclination angle, the inertia tensor of the front frame, and the rear and front suspensions is analyzed. The model presented, together with the linearized equations of motion obtained in this work, enables a systematic analysis of the stability of these vehicles, which helps design new electric kickscooters with improved vehicle safety conditions and oriented to a wider range of potential users.

Keywords Electric kickscooter · Nonholonomic system · Linearization · Stability analysis

1 Introduction

Personal transportation in urban areas has been evolving in recent years, with more and more people increasingly opting for light and nonpolluting means of transport. Among the

✉ A.G. Agúndez
  agarciaagundez@us.es

  D. García-Vallejo
  dgvallejo@us.es

  E. Freire
  efrem@us.es

¹ Department of Mechanical Engineering and Manufacturing, Universidad de Sevilla, Sevilla, Spain

² Department of Applied Mathematics II, Universidad de Sevilla, Sevilla, Spain

 Springer

advantages that users find are economic savings, physical exercise, and respect for the environment [1]. In addition to these advantages, there is a growing problem in the centers of large and medium-sized cities, where the high number of motorized vehicles causes high pollution and permanent traffic jams. Many municipalities have already limited the use of combustion-engine vehicles in city centers, and this restriction is expected to become increasingly widespread and restrictive. Therefore, the use of light, nonpolluting, single-person vehicles such as bicycles or scooters is emerging as a widely used alternative. Moreover, the use of these vehicles is being boosted introducing electric motors. Electric bicycles and scooters allow covering longer distances (or with greater slopes) while reducing the required physical effort of the rider, thus making them accessible to more people. Among the light unipersonal electric vehicles, one can find the bicycle, the scooter, the Segway, or the skateboard, with the electric bicycle being the most widespread among them. However, given its lightness, small size, and low physical effort required, the electric kickscooter (hereafter referred to as an e-scooter) is presented as a present and future alternative to the bicycle.

In vehicle dynamics, bicycles and motorcycles have been research subjects for more than 120 years. The work by Whipple [2], in 1899, was the first paper devoted to the stability analysis of bicycles. Linear and nonlinear dynamics aspects of a simplified bicycle model, together with some experiments, were presented by Åström et al. [3], and Limebeer et al. [4] considered simple and complex models to perform a review of different bicycle and motorcycle aspects. Meijaard et al. [5] presented, in 2007, a remarkable work with a well-acknowledged benchmark bicycle model with a complete list of validated parameters. This benchmark has been extensively used in several experimental [6] and theoretical works [7–10] devoted to multibody dynamics. The linear stability of the steady forward and circular motions of the bicycle benchmark was meticulously analyzed by Basu-Mandal et al. [7] and Xiong et al. [9, 11]. Furthermore, more advanced models of frames, tires, and riders were introduced in different extensions of the bicycle benchmark [12–17]. To describe the interaction of the electric drive components on the driving characteristics of electrically assisted bicycles, simulations of the driving behavior of bicycles with different positions of battery and motor in open- and closed-loop tests can be found by Bolk et al. [18]. With regard to motorcycles, Sharp [19] was one of the first authors to publish his stability studies by computing the eigenvalues of a motorcycle under different conditions, describing the three most characteristic linear modes of two-wheeled vehicles. Cooper [20] showed the importance of aerodynamic effects on the stability of motorcycles when traveling at high speeds, and Jennings [21] showed that the stability of a motorcycle is sensitive to suspension damping. Next, Sharp [22] studied the effect of accelerations and decelerations on stability, and Roe et al. [23] analyzed the effect of torsional stiffness on stability improvement. Splerings [24] studied the gyroscopic effect on stability, and Nishimi et al. [25] compared the frequencies and modes computed by eigenvalue calculation of a motorcycle model with those obtained with experimental modal analysis. A sensitivity analysis to assess the stability of the motorcycle, based on eigenvalue calculation and experimental work, was performed by Sharp [26]. The comparison of a modal analysis using eigenvalue computation and experimental results was also carried out by Cossalter et al. [27], and the stability analysis of a scooter was presented in [28].

The number of works devoted to the study of e-scooters has rapidly increased in recent years. The potential of e-scooters as a hybrid mode of transport, combined with public transport in large cities, was confirmed by Kostrzewska et al. [29]. Several studies related to safety and injuries exist. Unkuri et al. [30] focus on injuries in children and teenagers on e-scooters, and Griffin et al. [31] compare the severity of injuries in children (aged 2–12

years) between traditional and motorized scooters. Mebert [32] carried out in Switzerland a study on injuries in adults aged 16-80 years, showing that the number of cases has increased in recent years. In the same way, a recent review performed by Kowalczewska et al. [33] concluded the rising number of accidents and injuries involving e-scooters. Moreover, the analysis of the stability and maneuverability of these vehicles to ensure the safety of the driver and other road users can be found in other works. García-Vallejo et al. [34] presented an e-scooter benchmark based on the SEAT eXS Kickscooter ES2, with its corresponding set of parameters. Using the linear equations of the bicycle benchmark by Meijaard et al. [5], in [34], it was shown that, for the numerical values of the presented e-scooter benchmark parameters, these vehicles are completely unstable in the velocity range 0–10 m/s. Next, Paudel et al. [35] presented the range of design parameters in the current designs of e-scooters and analyzed their performance in terms of self-stability, braking effect, and steady-state turning. Despite finding some self-stability velocity range, the results showed that the current e-scooter designs are not as stable as bicycles, and these vehicles were found unstable within the most common range of legislated riding velocity. Klinger et al. [36] carried out simulation studies and on-road tests for two scenarios of particular interest from a vehicle safety perspective: straight-line stability and emergency braking. Concerning the driver's comfort, Asperti et al. [37] studied the vertical dynamic behavior by presenting a model that accounts for the mechanical impedance of the driver, and Cano-Moreno et al. [38] quantitatively assessed, based on the velocity and quality of the road, the effects of vibrations on the comfort and health of the e-scooter driver. Garman et al. [39], by designing a test course simulating an urban environment, performed a successful characterization of the e-scooter rider kinematics and vehicle dynamics. Brunner et al. [40] analyzed the impact of hand signals and rear blind spot checks on e-scooters stability, and Dozza et al. [41] introduced a framework for a data-driven evaluation of micro-mobility vehicles (bicycles and e-scooters) in field tests. Nevertheless, to the best of authors' knowledge, a detailed e-scooter multibody model for methodologically analyzing the stability of these vehicles has not yet been presented.

The objectives of this paper are to present a detailed multibody model of an e-scooter, obtain the linearized equations along the steady forward motion as a function of the main design parameters of the vehicle, and conduct a detailed linear stability analysis. The paper presents several contributions. First, an e-scooter multibody model, which considers the numerical values of the e-scooter benchmark by García-Vallejo et al. [34] and is based on the SEAT eXS Kickscooter ES2, is presented. First, compared to previous works existing in the literature, the model includes toroidal wheels instead of hoop-shaped wheels and rear and front suspensions. Second, another major contribution is the derivation of the reduced linearized equations of motion of the uncontrolled e-scooter multibody model along the steady forward motion. In the works by García-Vallejo et al. [34] and Paudel et al. [35], the linear stability analysis is conducted using the linear lean and steer equations of the bicycle benchmark by Meijaard et al. [5], which involve ad hoc linearization as opposed to linearization of fully nonlinear equations. The linearized equations by Meijaard et al. [5], based on the work by Papadopoulos [42], are derived using angular momentum balance about various axes and are not based on a systematic linearization of fully nonlinear equations of motion. In contrast, this paper develops a detailed nonlinear model of the e-scooter. An efficient linearization approach [43], previously used with the bicycle benchmark [43] and the waveboard [44] multibody models, is used in this work. With this linearization approach, the analytical expressions of the linearized equations are obtained not only as a function of the geometric and inertial parameters of the benchmark by Meijaard et al. [5] but also as a function of the toroidal wheels' and suspensions' parameters of the e-scooter.

Lastly, since the eigenvalues are parameterized in terms of these design parameters, a detailed linear stability analysis is performed by considering a wide range of scenarios. In this way, studying the influence of the different design parameters on the stability of these vehicles will help develop new e-scooters with improved vehicle safety conditions and oriented to a wider range of potential users, including elderly and physically impaired individuals.

The following structure is considered. After the Introduction part, Sect. 2 describes the e-scooter multibody model in detail. Particular attention is paid to describing the model of toroidal wheels and the front and rear suspensions, and the nonlinear equations of motion are derived. Next, Sect. 3 presents the linearized equations of motion along the steady forward motion. In Sect. 4, the linear stability results are shown and discussed, and finally, Sect. 5 summarizes the main conclusions obtained from this work.

2 Description of the e-scooter multibody model

In this section, the e-scooter multibody model is presented. The model considers the geometric and dynamic parameters of the e-scooter benchmark proposed by García-Vallejo et al. [34], corresponding to the SEAT eXS Kickscooter ES2. The modeling of the toroidal wheels and the rear and front suspensions are described in detail, and the nonlinear equations of motion are presented.

2.1 Description of the multibody model

The multibody model presents seven rigid bodies: the rear and front wheels are bodies R and F, respectively; the rear body and frame assembly, which includes a rigid rider, is body B; the front handlebar is designated as body H; the rear and front suspensions are represented as bodies S_R and S_F, respectively; and lastly, the global reference frame is denoted as body 1. The origin of the global frame is O_1, and the origins of the body reference frames are located at the respective centres of mass G_j, with $j = \{R, F, B, H, S_R, S_F\}$.

To describe the system, a set of $n = 15$ coordinates is used, with the $n \times 1$ vector of coordinates $\boldsymbol{x}$ given by:

$$\boldsymbol{x} = \begin{pmatrix} x_b & y_b & z_b & \psi_b & \phi_b & \theta_b & \delta & s & \theta_{S_R} & \theta_R & \theta_F & \xi_R & \xi_F & \eta_R & \eta_F \end{pmatrix}^{\mathrm{T}}. \quad (1)$$

The coordinates x_b, y_b, and z_b are Cartesian coordinates that locate the centre of mass G_B; ψ_b is the yaw angle; ϕ_b is the lean angle; and θ_b is the pitch angle. The triplet $\{\psi_b, \phi_b, \theta_b\}$ allows orientating body B in space. The steering angle δ corresponds to the rotation of the handlebar with respect to body B. The coordinate s represents the distance between G_H and G_F and considers the spring elongation of the front suspension, and θ_{S_R} represents the rotation of body S_R with respect to body B, due to the rear suspension. The rotations of the rear and front wheels are given by θ_R and θ_F, respectively. Lastly, ξ_R, ξ_F, η_R and η_F are angular coordinates used to describe the toroidal geometry of the wheels. Figure 1 shows the numbering of the bodies, the set of generalized coordinates of the system and the body reference frames, and a lateral view of the multibody model with the main geometric parameters is depicted in Fig. 2.

The list of parameters of the e-scooter, classified into geometric, dynamic, wheels' and suspensions' parameters, is shown in Table 1 of Appendix A. The numerical values of these parameters correspond to those of the SEAT eXS Kickscooter ES2. To obtain the moment
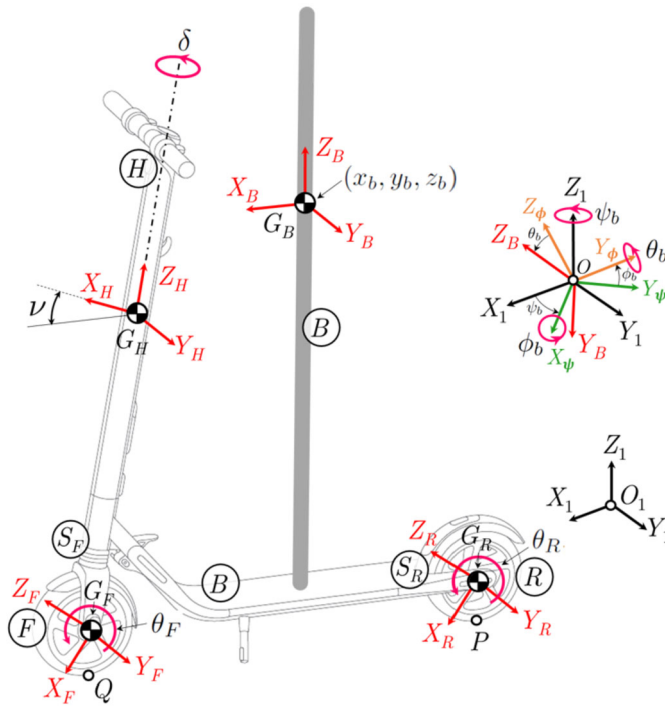
Fig. 1 Multibody model of the SEAT eXS Kickscooter ES2: numbering of the bodies and body reference frames. The generalized coordinates of the multibody system, presented in Eq. (1), are shown, except for the coordinate θ_{S_R}, shown in Fig. 4 (b); the coordinate s, depicted in Fig. 5 (b); and the angular coordinates ξ_R, ξ_F, η_R and η_F, which are shown in detail in Fig. 6. The rigid rider is represented in a simplified manner to facilitate the visualization of the multibody model

of inertia tensors of the bodies, a CAD model of the e-scooter, shown in Fig. 3, is created. Figure 3 (a) shows a view of the e-scooter without including the rider, and Fig. 3 (b) depicts the vehicle with the rider model. A rigid rider with mass $m_h = 75$ kg is considered in this work. As detailed in Table 1 of Appendix A, the mass of body B includes the masses of the deck, $m_d = 2.5$ kg, and the rider, and is given by $m_B = m_d + m_h = 77.5$ kg. Note that, in Figs. 1 and 2, the shape of the rider has been simplified in order to ease the visualization of the multibody model. The orientation matrices of the body reference frames, expressed as a function of the elemental rotation matrices, are given by:

$$R_B(x) = R_{\psi_b} R_{\phi_b} R_{\theta_b}, \qquad R_{S_R}(x) = R_B R_{\theta_{S_R}}, \qquad R_R(x) = R_{S_R} R_{\theta_R}, \qquad (2)$$

$$R_H(x) = R_B R_\nu R_\delta, \qquad R_{S_F}(x) = R_H, \qquad R_F(x) = R_{S_F} R_{\theta_F}, \qquad (3)$$

where R_ν considers the steer axis tilt angle denoted by ν in Fig. 1.

A detailed view of the rear suspension is shown in Fig. 4. In particular, Fig. 4 (a) shows a view of the rear suspension of a SEAT eXS Kickscooter ES2, and Fig. 4 (b) illustrates a scheme with body S_R and the coordinate θ_{S_R}. Note that, as shown in Fig. 4 (b), the rear suspension is modeled by means of a torsion spring, with stiffness constant k_r, and a damper with damping coefficient d_r. Similarly, Fig. 5 (a) shows the front suspension of the SEAT
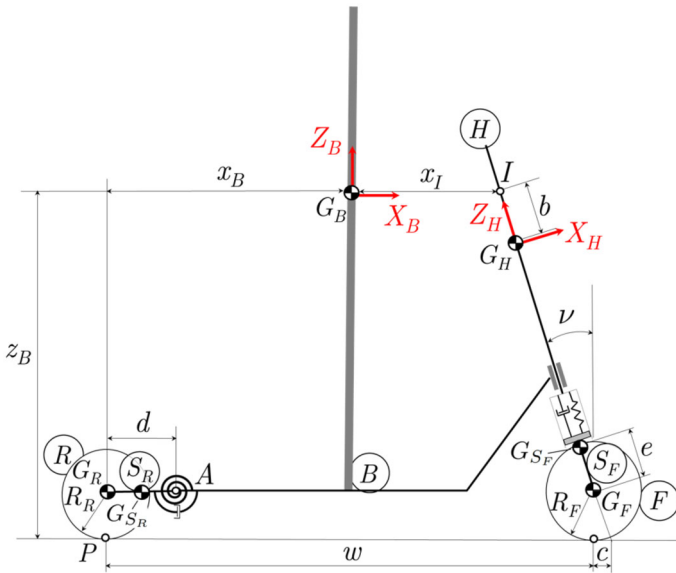
Fig. 2 Lateral view of the e-scooter multibody model with the main geometric parameters. A detailed list of the parameters with their numerical values can be found in Table 1 of Appendix A
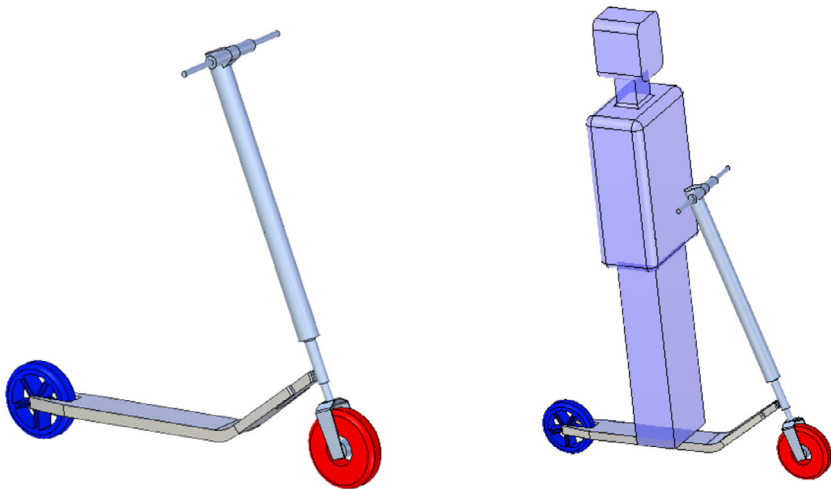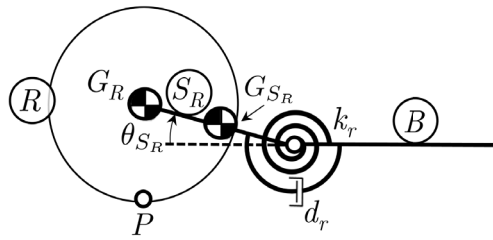

(a) CAD model of the SEAT eXS Kickscooter ES2   (b) CAD model including the rider

Fig. 3 CAD model of the e-scooter SEAT eXS Kickscooter ES2, with a rigid rider of mass $m_h = 75$ kg

eXS Kickscooter ES2, and Fig. 5 (b) presents a scheme with body S_F and the coordinate s. The front suspension is modeled as a linear spring with stiffness constant k_f and a damper with damping coefficient d_f.
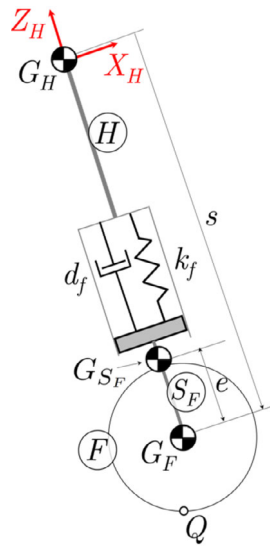
(a) Rear suspension of the SEAT eXS Kickscooter ES2

(b) Detail of body S_R, rear suspension and coordinate θ_{S_R}

Fig. 4 Rear suspension of the e-scooter multibody model

(a) Front suspension of the SEAT eXS Kickscooter ES2

(b) Detail of body S_F, front suspension and coordinate s

Fig. 5 Front suspension of the e-scooter multibody model

The position vectors of the centres of mass G_j, expressed in the global reference frame, are computed as follows:

$$
\begin{aligned}
&\boldsymbol{r}_{G_B} = \begin{pmatrix} x_b & y_b & z_b \end{pmatrix}^{\mathrm{T}}, && \boldsymbol{r}_A = \boldsymbol{r}_{G_B} + \boldsymbol{R}_B \bar{\boldsymbol{r}}_{G_B A}, \\
&\boldsymbol{r}_{G_{S_R}} = \boldsymbol{r}_A + \boldsymbol{R}_{S_R} \bar{\boldsymbol{r}}_{A G_{S_R}}, && \boldsymbol{r}_{G_R} = \boldsymbol{r}_A + \boldsymbol{R}_{S_R} \bar{\boldsymbol{r}}_{A G_R}, \\
&\boldsymbol{r}_I = \boldsymbol{r}_{G_B} + \boldsymbol{R}_B \bar{\boldsymbol{r}}_{G_B I}, && \boldsymbol{r}_{G_H} = \boldsymbol{r}_I + \boldsymbol{R}_H \bar{\boldsymbol{r}}_{I G_H}, \\
&\boldsymbol{r}_{G_F} = \boldsymbol{r}_{G_H} + \boldsymbol{R}_H \bar{\boldsymbol{r}}_{G_H G_F}, && \boldsymbol{r}_{G_{S_F}} = \boldsymbol{r}_{G_F} + \boldsymbol{R}_H \bar{\boldsymbol{r}}_{G_F G_{S_F}},
\end{aligned}
\tag{4}
$$

where r_A and r_I are the position vectors of points A and I, shown in Fig. 2. In Eqs. (4), $\bar{r}_{G_B A}$, $\bar{r}_{AG_{S_R}}$, $\bar{r}_{AG_R}$, $\bar{r}_{G_B I}$, $\bar{r}_{IG_H}$, $\bar{r}_{G_H G_F}$ and $\bar{r}_{G_F G_{S_F}}$ are vectors, expressed in the body reference frames, given by:

$$\bar{r}_{G_B A} = \begin{pmatrix} d - x_B & 0 & R_R - z_B \end{pmatrix}^{\mathrm{T}}, \qquad \bar{r}_{AG_{S_R}} = \begin{pmatrix} -d/2 & 0 & 0 \end{pmatrix}^{\mathrm{T}},$$

$$\bar{r}_{AG_R} = \begin{pmatrix} -d & 0 & 0 \end{pmatrix}^{\mathrm{T}}, \qquad \bar{r}_{G_B I} = \begin{pmatrix} x_I & 0 & 0 \end{pmatrix}^{\mathrm{T}}, \qquad (5)$$

$$\bar{r}_{IG_H} = \begin{pmatrix} 0 & 0 & -b \end{pmatrix}^{\mathrm{T}}, \qquad \bar{r}_{G_H G_F} = \begin{pmatrix} 0 & 0 & -s \end{pmatrix}^{\mathrm{T}},$$

$$\bar{r}_{G_F G_{S_F}} = \begin{pmatrix} 0 & 0 & e \end{pmatrix}^{\mathrm{T}},$$

where x_B and z_B are the horizontal and vertical distances, respectively, between the centre of mass G_B and the rear contact point P; x_I is the horizontal distance between G_B and the auxiliar point I; b is the distance between I and the centre of mass G_H; d is the distance between the auxiliar point A and the centre of mass G_R; e is the distance between G_F and G_{S_F}; and R_R is the radius of the rear wheel. These parameters are shown in Fig. 2, and their numerical values are presented in Appendix A.

2.2 Description of the toroidal wheels

The wheels of the e-scooter are modeled as tori with elliptic cross-section. To parameterize the surfaces of the toroidal wheels, the angular coordinates ξ_i and η_i, presented in Eq. (1), with $i = \{R, F\}$, are used. The toroidal wheels present a major radius ρ_i and a minor radius a_i, verifying the following relation:

$$\rho_i + a_i = R_i, \qquad (6)$$

where R_i is the radius of the hoop-shaped wheel of equivalent radius.

In the elliptic cross-section, the minor axis of the ellipse is b_i, and the major axis corresponds to the previously mentioned minor radius of the torus a_i. The elliptic profile r_i, in polar form relative to its centre, is given by:

$$r_i (\eta_i) = \frac{a_i b_i}{\sqrt{(b_i \cos (\eta_i))^2 + (a_i \sin (\eta_i))^2}}. \qquad (7)$$

Note that the elliptic profile is parameterized in terms of the coordinate η_i. Figure 6 (a) presents a three-dimensional view of the toroidal wheel, with the coordinates ξ_i and η_i, and Fig. 6 (b) represents a cross-section of the wheel, where the geometric parameters ρ_i, a_i, and b_i can be seen.

The geometry of the wheel is completely described by defining the nondimensional parameters μ_i and σ_i, with $i = \{R, F\}$:

$$\mu_i = \frac{a_i}{\rho_i}, \qquad \sigma_i = \frac{b_i}{a_i}, \qquad (8)$$

where μ_i is the torus aspect ratio, given by the ratio of the minor to the major radius of the wheel, and σ_i is the aspect ratio of the elliptical cross-section, defined as the ratio of the minor to the major radius of the ellipse. Note that the hoop-shaped wheel case of the e-scooter benchmark in Ref. [34] is also captured with this model and is obtained by degenerating the tori for $\mu_i = \sigma_i = 0$, leading to $\rho_i = R_i$. The inertia tensors of the rear and front wheels used

(a) Three-dimensional view of the toroidal wheel

(b) Cross-section of the toroidal wheel
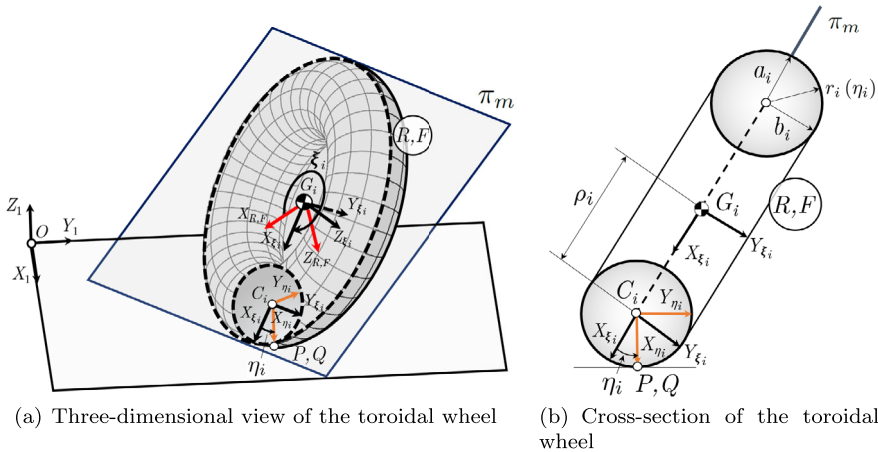
Fig. 6 Model of the toroidal wheel. A three-dimensional view of the wheel is shown in Fig. 6 (a), which depicts the angular coordinates ξ_i and η_i, with $i = \{R, F\}$, that describe the toroidal geometry. The local reference frames, the centre of mass G_i, the centre of the torus tube C_i, and the contact points with the ground, denoted as P and Q for the rear and front wheels, respectively, are also shown in Fig. 6 (a). A cross-section of the wheel is depicted in Fig. 6 (b), illustrating the major radius of the torus, ρ_i, and the minor and major axes of the elliptic cross-section, b_i and a_i, respectively

in the e-scooter benchmark [34] are substituted by the inertia tensors of an elliptic torus, parameterized in terms of the cross-section parameters ρ_i, a_i, and b_i, whose expressions can be found by Diaz et al. [45]:

$$I_{i_{xx}} = I_{i_{zz}} = \frac{1}{8} m_i \left(4\rho_i^2 + 3a_i^2 + 2b_i^2 \right), \tag{9}$$

$$I_{i_{yy}} = \frac{1}{4} m_i \left(4\rho_i^2 + 3a_i^2 \right), \tag{10}$$

with $i = \{R, F\}$.

The contact of the e-scooter wheels with the ground leads to the following set of holonomic constraints:

$$C(x) = \begin{pmatrix} r_{P_Z} & r_{Q_Z} & \mathbf{n} \cdot \mathbf{t}_{L_R} & \mathbf{n} \cdot \mathbf{t}_{T_R} & \mathbf{n} \cdot \mathbf{t}_{L_F} & \mathbf{n} \cdot \mathbf{t}_{T_F} \end{pmatrix}^{\mathrm{T}} = \mathbf{0}, \tag{11}$$

where r_{P_Z} and r_{Q_Z} are the Z-components of the position vectors of the contact points, $\mathbf{r}_P$ and $\mathbf{r}_Q$; $\mathbf{t}_{L_i}$ and $\mathbf{t}_{T_i}$ are the longitudinal and transversal tangent vectors to the contact points; and $\mathbf{n}$ is the normal vector to the ground surface. These vectors are given by:

$$\mathbf{r}_P = \mathbf{r}_{G_R} + \mathbf{R}_R \bar{\mathbf{r}}_{G_R P}, \qquad \mathbf{r}_Q = \mathbf{r}_{G_F} + \mathbf{R}_F \bar{\mathbf{r}}_{G_F Q},$$

$$\mathbf{t}_{L_R} = \mathbf{R}_R \frac{\partial \bar{\mathbf{r}}_{G_R P}}{\partial \xi_R}, \qquad \mathbf{t}_{T_R} = \mathbf{R}_R \frac{\partial \bar{\mathbf{r}}_{G_R P}}{\partial \eta_R}, \tag{12}$$

$$\mathbf{t}_{L_F} = \mathbf{R}_F \frac{\partial \bar{\mathbf{r}}_{G_F Q}}{\partial \xi_F}, \qquad \mathbf{t}_{T_F} = \mathbf{R}_F \frac{\partial \bar{\mathbf{r}}_{G_F Q}}{\partial \eta_F}.$$

In Eqs. (12), $\bar{r}_{G_R P}$ and $\bar{r}_{G_F Q}$ are position vectors, expressed in the local reference frames of bodies R and F, respectively, and computed as follows:

$$\bar{r}_{G_R P} = R_{\xi_R} \left(\rho_R + R_{\eta_R} r_R \right), \qquad \bar{r}_{G_F Q} = R_{\xi_F} \left(\rho_F + R_{\eta_F} r_F \right),$$

$$\rho_R = \begin{pmatrix} \rho_R & 0 & 0 \end{pmatrix}^{\mathrm{T}}, \qquad \rho_F = \begin{pmatrix} \rho_F & 0 & 0 \end{pmatrix}^{\mathrm{T}},$$

$$r_R = \begin{pmatrix} r_R(\eta_R) & 0 & 0 \end{pmatrix}^{\mathrm{T}}, \qquad r_F = \begin{pmatrix} r_F(\eta_F) & 0 & 0 \end{pmatrix}^{\mathrm{T}}, \qquad (13)$$

where R_{ξ_i} and R_{η_i} are the rotation matrices corresponding to the coordinates ξ_i and η_i.

The wheels are assumed to roll without slipping, which leads to the following nonholonomic constraints:

$$C_{nh}(x, \dot{x}) = \begin{pmatrix} v_{P_x} & v_{P_y} & v_{Q_x} & v_{Q_y} \end{pmatrix}^{\mathrm{T}} = \mathbf{0}. \qquad (14)$$

In Eq. (14), v_P and v_Q are the velocity of the contact points P and Q, respectively, computed as follows:

$$v_P = v_{G_R} + R_R \left(\bar{\omega}_R \times \bar{r}_{G_R P} \right), \qquad v_Q = v_{G_F} + R_F \left(\bar{\omega}_F \times \bar{r}_{G_F Q} \right), \qquad (15)$$

where v_{G_R} and v_{G_F} are the absolute velocities of G_R and G_F, and $\bar{\omega}_R$ and $\bar{\omega}_F$ are the angular velocities of the rear and front wheels, respectively, expressed in the local reference frames of bodies R and F.

Therefore, the e-scooter multibody model presents $n = 15$ coordinates, $m = 6$ holonomic constraints and $l = 4$ nonholonomic constraints, which results in $n_g = n - m - l = 5$ degrees of freedom.

2.3 Description and characterization of the suspensions

As shown in Fig. 4 (b), the model of the rear suspension consists of a torsion spring and damper, with stiffness constant k_r and damping coefficient d_r, respectively. The torques acting on bodies B and S_R due to the rear suspension, expressed in the corresponding body reference frames, are given by:

$$\bar{M}^B = \bar{M}_e^B + \bar{M}_d^B, \qquad \bar{M}^{S_R} = -\bar{M}^B, \qquad (16)$$

where $\bar{M}_e^B$ is the elastic torque due to the torsion spring, and $\bar{M}_d^B$ is the torque due to the damper:

$$\bar{M}_e^B = \begin{pmatrix} 0 & k_r \left(\theta_{S_R} - \theta_{S_R}^* \right) & 0 \end{pmatrix}^{\mathrm{T}}, \qquad \bar{M}_d^B = \begin{pmatrix} 0 & d_r \dot{\theta}_{S_R} & 0 \end{pmatrix}^{\mathrm{T}}. \qquad (17)$$

In Eq. (17), $\theta_{S_R}^*$ is the value of the coordinate θ_{S_R} when the torsion spring presents its natural length. In the present work, it is assumed that $\theta_{S_R}^* = 0°$.

The generalized force vectors associated with the torques $\bar{M}^B$ and $\bar{M}^{S_R}$ are obtained as:

$$Q_B = G_B^{\mathrm{T}} \bar{M}^B, \qquad Q_{S_R} = G_{S_R}^{\mathrm{T}} \bar{M}^{S_R}, \qquad (18)$$

where the matrices G_B and G_{S_R} are computed as follows:

$$G_B = \frac{\partial \bar{\omega}_B}{\partial \dot{x}}, \qquad G_{S_R} = \frac{\partial \bar{\omega}_{S_R}}{\partial \dot{x}}. \qquad (19)$$

In Eq. (19), $\bar{\boldsymbol{\omega}}_B$ and $\bar{\boldsymbol{\omega}}_{S_R}$ are the angular velocities of bodies B and S_R, respectively, expressed in their corresponding body frames.

With regard to the front suspension, the model consists of a linear spring and a damper, with stiffness constant k_f and damping coefficient d_f. The forces acting on bodies H and S_F due to the front suspension, expressed in the global frame, are denoted as $\boldsymbol{F}_H$ and $\boldsymbol{F}_{S_F}$, respectively, and computed as follows:

$$\boldsymbol{F}_H = \boldsymbol{R}_H \left(\bar{\boldsymbol{F}}_e^H + \bar{\boldsymbol{F}}_d^H \right), \qquad\qquad \boldsymbol{F}_{S_F} = -\boldsymbol{F}_H, \qquad (20)$$

where $\bar{\boldsymbol{F}}_e^H$ is the elastic force, and $\bar{\boldsymbol{F}}_d^H$ is the damping force. The expressions of $\bar{\boldsymbol{F}}_e^H$ and $\bar{\boldsymbol{F}}_d^H$, expressed in the body frame H, are given by:

$$\bar{\boldsymbol{F}}_e^H = \begin{pmatrix} 0 & 0 & -k_f \left(s - s^* \right) \end{pmatrix}^{\mathrm{T}}, \qquad \bar{\boldsymbol{F}}_d^H = \begin{pmatrix} 0 & 0 & -d_f \dot{s} \end{pmatrix}^{\mathrm{T}}. \qquad (21)$$

In Eq. (21), s^* is the value of the coordinate s when the spring presents its natural length. In the present work, s^* is computed as follows:

$$s^* = l - b, \qquad (22)$$

where b was defined after Eq. (5), and l is the distance between the auxiliar point I, shown in Fig. 2, and the centre of mass G_F in the rigid case. The expression of l can be found in Appendix A.

The generalized force vectors associated with the forces $\boldsymbol{F}_H$ and $\boldsymbol{F}_{S_F}$ are given by:

$$\boldsymbol{Q}_H = \boldsymbol{H}_H^{\mathrm{T}} \boldsymbol{F}_H, \qquad\qquad \boldsymbol{Q}_{S_F} = \boldsymbol{H}_{S_F}^{\mathrm{T}} \boldsymbol{F}_{S_F}, \qquad (23)$$

where the matrices $\boldsymbol{H}_H$ and $\boldsymbol{H}_{S_F}$ are computed as follows:

$$\boldsymbol{H}_H = \frac{\partial \boldsymbol{r}_{G_H}}{\partial \boldsymbol{x}}, \qquad\qquad \boldsymbol{H}_{S_F} = \frac{\partial \boldsymbol{r}_{G_{S_F}}}{\partial \boldsymbol{x}}. \qquad (24)$$

To obtain the numerical values of the stiffness constants k_r, k_f and the damping coefficients d_r, d_f, a series of tests have been carried out. To this end, a special test bed was built in the laboratory of Mechanical Engineering of the University of Seville; see Fig. 7 (a). The stiffness and damping constants were obtained by conducting quasi-static and dynamic tests, respectively. The loads were applied using a servo-hydraulic axial actuator, which was controlled by software. The load capacity of the actuator and the load cell was 12 kN. The load was applied using a spherical joint over a rigid flat surface (Fig. 7 (b)) to avoid moments at the load application points and, at the same time, uniformly distribute the load at the applied section. Figures 7 (c) and (d) show the e-scooter during the tests, with the load being applied at different locations. The tests provided the following results:

$$k_f = 122.05 \text{ N/mm}, \qquad\qquad d_f = 221.61 \text{ N s/m}, \qquad (25)$$

$$k_r = 1202.18 \text{ Nm/rad}, \qquad\qquad d_r = 12.28 \text{ Nm/(rad/s)}. \qquad (26)$$

Table 1 summarizes the geometric, inertial, wheels' and suspensions' parameters of the e-scooter multibody model, with their corresponding numerical values. It is important to note that these numerical values correspond to the SEAT eXS Kickscooter ES2. Currently, the numerical values of the parameters vary due to the existence of numerous e-scooter designs. These design differences result in variability in scooter performance as well as overall rider experience.

a)   b)

c)   d)
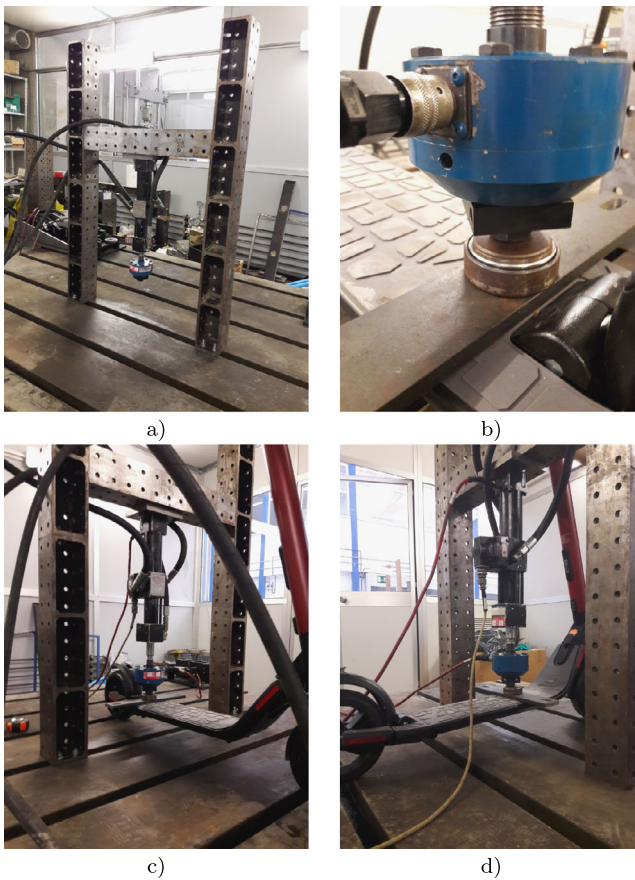
Fig. 7 Pictures of the e-scooter during the quasi-static and dynamic tests for stiffness and damping parameter estimation: (a) test bed built for stiffness and damping tests; (b) details of the load cell and spherical joint, c) e-scooter during the tests with the load applied close to rear axis; and (d) e-scooter during the tests with the load applied close to front axis

2.4 Equations of motion of the e-scooter multibody model

The equations of motion of the e-scooter are given by the dynamic equations, which are derived as explained by Schiehlen [46]; the holonomic constraints (11); and the nonholonomic constraints (14), leading to the following index-3 Differential-Algebraic Equations (DAE) system:

$$M(x)\ddot{x} + D^{\mathrm{T}}(x)\Lambda = Q(x,\dot{x}) + Q_{\mathrm{ext}}(x),\qquad(27)$$

$$C(x) = 0,\qquad(28)$$

$$C_{nh}(x,\dot{x}) = B(x)\dot{x} = 0.\qquad(29)$$

In Eqs. (27)–(29), Λ is the $(m+l)\times 1$ vector of Lagrange multipliers; $M(x)$ is the $n\times n$ mass matrix; and $B(x)$ and $D(x)$ are $l\times n$ and $(m+l)\times n$ matrices, respectively, computed

as:

$$B\left(x\right) = \frac{\partial C_{nh}\left(x, \dot{x}\right)}{\partial \dot{x}}, \quad D\left(x\right) = \begin{pmatrix} C_x\left(x\right) \\ B\left(x\right) \end{pmatrix}, \tag{30}$$

where $C_x = \frac{\partial C}{\partial x}$. Moreover, in Eq. (27), $Q\left(x, \dot{x}\right)$ is the $n \times 1$ vector of generalized forces, given by:

$$Q\left(x, \dot{x}\right) = Q_g\left(x\right) + Q_v\left(x, \dot{x}\right) + Q_B\left(x, \dot{x}\right) + Q_{S_R}\left(x, \dot{x}\right)$$
$$+ Q_H\left(x, \dot{x}\right) + Q_{S_F}\left(x, \dot{x}\right), \tag{31}$$

where $Q_g\left(x\right)$ is the generalized gravity force vector; $Q_v\left(x, \dot{x}\right)$ is the quadratic-velocity inertia term, associated with the inertia forces that are quadratic with respect to the system velocities (centrifugal and Coriolis forces); and $Q_B\left(x, \dot{x}\right)$, $Q_{S_R}\left(x, \dot{x}\right)$, $Q_H\left(x, \dot{x}\right)$ and $Q_{S_F}\left(x, \dot{x}\right)$ are the generalized force vectors due to the rear and front suspensions, presented in Eqs. (18) and (23). Lastly, in Eq. (27), $Q_{\text{ext}}\left(x\right)$ is the $n \times 1$ vector of generalized forces due to the external actuations exerted by the rider.

3 Linearization of the equations of motion

In this section, the steady forward motion of the uncontrolled e-scooter (considering $Q_{\text{ext}}\left(x\right) = 0$) is described, and the linearized equations of motion along this reference motion are derived.

3.1 Description of the reference motion

The steady forward motion of the e-scooter is expressed as:

$$x^0 = \begin{pmatrix} x_b^0 & y_b^0 & z_b^0 & \psi_b^0 & \phi_b^0 & \theta_b^0 & s^0 & \theta_{S_R}^0 & \theta_R^0 & \theta_F^0 & \xi_R^0 & \xi_F^0 & \eta_R^0 & \eta_F^0 \end{pmatrix}^{\text{T}}, \tag{32}$$

with

$$
\begin{aligned}
&x_b^0\left(t\right) = vt, &\quad &\theta_{S_R}^0\left(t\right) = \theta_{S_R}^0, \\
&y_b^0\left(t\right) = 0, &\quad &\theta_R^0\left(t\right) = \frac{v}{R_R}t, \\
&z_b^0\left(t\right) = z_0, &\quad &\theta_F^0\left(t\right) = \frac{v}{R_F}t, \\
&\psi_b^0\left(t\right) = 0, &\quad &\xi_R^0\left(t\right) = \zeta_R^0 - \theta_R^0\left(t\right), \\
&\phi_b^0\left(t\right) = 0, &\quad &\xi_F^0\left(t\right) = \zeta_F^0 - \theta_F^0\left(t\right), \\
&\theta_b^0\left(t\right) = \theta_0, &\quad &\eta_R^0\left(t\right) = 0, \\
&\delta^0\left(t\right) = 0, &\quad &\eta_F^0\left(t\right) = 0, \\
&s^0\left(t\right) = s_0. &\quad &
\end{aligned}
\tag{33}
$$

In Eqs. (33), v is the forward speed and z_0, θ_0, s_0, $\theta_{S_R}^0$, ζ_R^0 and ζ_F^0 are constants. The reference solution (32) verifies the equations of motion (27)–(29):

$$M\left(x^0\right)\ddot{x}^0 + D^{\mathrm{T}}\left(x^0\right)\Lambda^0 = Q\left(x^0, \dot{x}^0\right), \tag{34}$$

$$C\left(x^0\right) = 0, \tag{35}$$

$$C_{nh}\left(x^0, \dot{x}^0\right) = B\left(x^0\right)\dot{x}^0 = 0, \tag{36}$$

where Λ^0 is the vector of Lagrange multipliers in the reference motion.

First, using the first, second, third, and fifth of the holonomic constraints (35), the constants z_0, s_0, ζ_R^0 and ζ_F^0 are determined:

$$z_0 = f_1\left(\theta_0, \theta_{S_R}^0, p\right), \tag{37}$$

$$s_0 = f_2\left(\theta_0, \theta_{S_R}^0, p\right), \tag{38}$$

$$\zeta_R^0 = \frac{\pi}{2} - \theta_0 - \theta_{S_R}^0, \tag{39}$$

$$\zeta_F^0 = v + \frac{\pi}{2} - \theta_0, \tag{40}$$

where the functions f_1 and f_2 can be found in Appendix B, and p represents the set of parameters of the multibody model, summarized in Table 1.

In addition, the dynamic equations (34) allow obtaining the equilibrium values θ_0, $\theta_{S_R}^0$ and the Lagrange multipliers associated with this reference motion, Λ^0, with:

$$\Lambda^0 = \left(\Lambda_1^0 \quad \Lambda_2^0 \quad \mathbf{0}_{1\times 8}\right)^{\mathrm{T}}. \tag{41}$$

In Eq. (41), the nonzero values of Λ_1^0 and Λ_2^0 are obtained by solving the third and sixth dynamic equations (34):

$$\Lambda_1^0 = \frac{\chi_1\left(\theta_0, \theta_{S_R}^0, s_0, p\right)}{\chi_3\left(\theta_0, \theta_{S_R}^0, s_0, p\right)}, \tag{42}$$

$$\Lambda_2^0 = \frac{\chi_2\left(\theta_0, \theta_{S_R}^0, s_0, p\right)}{\chi_3\left(\theta_0, \theta_{S_R}^0, s_0, p\right)}. \tag{43}$$

Moreover, the equilibrium values θ_0 and $\theta_{S_R}^0$ are obtained from solving the following nonlinear system of equations:

$$f_3\left(\theta_0, \theta_{S_R}^0, p\right) = 0, \tag{44}$$

$$f_4\left(\theta_0, \theta_{S_R}^0, p\right) = 0, \tag{45}$$

where the functions χ_1, χ_2, χ_3, f_3 and f_4 can be found in Appendix B.

If the suspensions are infinitely rigid ($k_r \to \infty$, $k_f \to \infty$), the constants z_0, θ_0, $\theta_{S_R}^0$, s_0, ζ_R^0 and ζ_F^0 of Eqs. (33) verify:

$$z_0 = z_B, \qquad\qquad \theta_0 = 0,$$
$$\theta_{S_R}^0 = 0, \qquad\qquad s_0 = s^*, \tag{46}$$

$$\zeta_R^0 = \frac{\pi}{2}, \qquad\qquad \zeta_F^0 = \nu + \frac{\pi}{2}. \tag{47}$$

3.2 Computation of the linearized equations of motion

The linearization of the equations of motion (27)–(29) is performed along the steady forward motion (33). To this end, the linearization approach [43], which showed an excellent computational efficiency with the bicycle benchmark [43] and the waveboard [44] multibody models, is used.

The variations with respect to the reference solution $\tilde{x}$, $\dot{\tilde{x}}$, $\ddot{\tilde{x}}$ and $\tilde{\Lambda}$ are introduced:

$$\tilde{x} = x - x^0, \ \dot{\tilde{x}} = \dot{x} - \dot{x}^0, \ \ddot{\tilde{x}} = \ddot{x} - \ddot{x}^0, \ \tilde{\Lambda} = \Lambda - \Lambda^0. \tag{48}$$

Following Ref. [43], given that the multibody model presents $m = 6$ holonomic constraints, a coordinate partition of the vector x of $n = 15$ coordinates into $n - m = 9$ admissible position coordinates, grouped in x_a, and $m = 6$ dependent coordinates x_d, is made. The set of admissible position coordinates x_a spans the domain of admissible positions of the multibody system. This partition is represented as $x = \begin{pmatrix} x_a & x_d \end{pmatrix}^{\mathrm{T}}$. Furthermore, the $l = 4$ nonholonomic constraints allow the partition of the time derivative of the admissible position coordinates $\dot{x}_a$ in $l = 4$ dependent and $n - m - l = 5$ independent admissible velocities, given by the vectors $\dot{x}_{ad}$ and $\dot{x}_{ai}$, respectively, and therefore $\dot{x}_a = \begin{pmatrix} \dot{x}_{ai} & \dot{x}_{ad} \end{pmatrix}^{\mathrm{T}}$. The same partition can be used at position level, with the coordinate vector finally partitioned as $x = \begin{pmatrix} x_{ai} & x_{ad} & x_d \end{pmatrix}^{\mathrm{T}}$. Therefore, the vector of variations $\tilde{x}$ can be written as:

$$\tilde{x} = \begin{pmatrix} \tilde{x}_{ai} & \tilde{x}_{ad} & \tilde{x}_d \end{pmatrix}^{\mathrm{T}}. \tag{49}$$

A possible coordinate partition in the e-scooter multibody model is:

$$\tilde{x}_{ai} = \begin{pmatrix} \tilde{x}_b & \tilde{\phi}_b & \tilde{\delta} & \tilde{s} & \tilde{\theta}_{S_R} \end{pmatrix}^{\mathrm{T}}, \qquad \tilde{x}_{ad} = \begin{pmatrix} \tilde{y}_b & \tilde{\psi}_b & \tilde{\theta}_R & \tilde{\theta}_F \end{pmatrix}^{\mathrm{T}}, \tag{50}$$

$$\tilde{x}_d = \begin{pmatrix} \tilde{z}_b & \tilde{\theta}_b & \tilde{\xi}_R & \tilde{\xi}_F & \tilde{\eta}_R & \tilde{\eta}_F \end{pmatrix}^{\mathrm{T}},$$

where the Cartesian coordinate x_b, the lean angle ϕ_b, the steering angle δ and the coordinates s and θ_{S_R}, associated with the front and rear suspensions, respectively, have been chosen as independent coordinates, as many as number of degrees of freedom ($n_g = 5$).

The following linear ODE system is obtained:

$$\ddot{\tilde{x}}_{ai} = J_{21}\tilde{x}_{ai} + J_{22}\dot{\tilde{x}}_{ai} + J_{23}\tilde{x}_{ad}, \tag{51}$$

$$\dot{\tilde{x}}_{ad} = J_{31}\tilde{x}_{ai} + J_{32}\dot{\tilde{x}}_{ai} + J_{33}\tilde{x}_{ad}, \tag{52}$$

where the expressions of the matrices J_{21}, J_{22}, J_{23}, J_{31}, J_{32} and J_{33} can be found in Ref. [43]. Defining $\tilde{X} = \begin{pmatrix} \tilde{x}_{ai} & \dot{\tilde{x}}_{ai} & \tilde{x}_{ad} \end{pmatrix}^{\mathrm{T}}$, the linearized equations of motion (51)-(52) can be written as a first-order system of the form:

$$\dot{\tilde{X}} = J\tilde{X}, \tag{53}$$

where J is the resulting Jacobian matrix built as follows:

$$J = \begin{pmatrix} \mathbf{0}_{(n-m-l)} & \mathbf{I}_{(n-m-l)} & \mathbf{0}_{(n-m-l)\times l} \\ \hline J_{21} & J_{22} & J_{23} \\ \hline J_{31} & J_{32} & J_{33} \end{pmatrix}. \tag{54}$$

The size of the Jacobian matrix $\boldsymbol{J}$ in Eq. (54) is $(2n - 2m - l) \times (2n - 2m - l) = 14 \times 14$. Therefore, the linearized equations of motion of the e-scooter are given by the following fourteen equations:

$$\dot{\tilde{x}}_b = \tilde{v}_{x_b}, \tag{55}$$

$$\dot{\tilde{\phi}}_b = \tilde{\omega}_{\phi_b}, \tag{56}$$

$$\dot{\tilde{\delta}} = \tilde{\omega}_\delta, \tag{57}$$

$$\dot{\tilde{s}} = \tilde{v}_s, \tag{58}$$

$$\dot{\tilde{\theta}}_{S_R} = \tilde{\omega}_{\theta_{S_R}}, \tag{59}$$

$$\dot{\tilde{v}}_{x_b} = \varrho_1 \tilde{s} + \varrho_2 \tilde{\theta}_{S_R} + \varrho_3 \tilde{v}_s + \varrho_4 \tilde{\omega}_{\theta_{S_R}}, \tag{60}$$

$$\dot{\tilde{\omega}}_{\phi_b} = \varrho_5 \tilde{\phi}_b + \left(\varrho_6 + \varrho_7 v^2\right) \tilde{\delta} + \varrho_8 v \tilde{\omega}_{\phi_b} + \varrho_9 v \tilde{\omega}_\delta, \tag{61}$$

$$\dot{\tilde{\omega}}_\delta = \varrho_{10} \tilde{\phi}_b + \left(\varrho_{11} + \varrho_{12} v^2\right) \tilde{\delta} + \varrho_{13} v \tilde{\omega}_{\phi_b} + \varrho_{14} v \tilde{\omega}_\delta, \tag{62}$$

$$\dot{\tilde{v}}_s = \varrho_{15} \tilde{s} + \varrho_{16} \tilde{\theta}_{S_R} + \varrho_{17} \tilde{v}_s + \varrho_{18} \tilde{\omega}_{\theta_{S_R}}, \tag{63}$$

$$\dot{\tilde{\omega}}_{\theta_{S_R}} = \varrho_{19} \tilde{s} + \varrho_{20} \tilde{\theta}_{S_R} + \varrho_{21} \tilde{v}_s + \varrho_{22} \tilde{\omega}_{\theta_{S_R}}, \tag{64}$$

$$\dot{\tilde{y}}_b = \gamma_1 v \tilde{\delta} + \gamma_2 \tilde{\omega}_{\phi_b} + \gamma_3 \tilde{\omega}_\delta + \gamma_4 v \tilde{\psi}_b, \tag{65}$$

$$\dot{\tilde{\psi}}_b = \gamma_5 v \tilde{\delta} + \gamma_6 \tilde{\omega}_\delta, \tag{66}$$

$$\dot{\tilde{\theta}}_R = \gamma_7 \tilde{v}_{x_b} + \gamma_8 \tilde{v}_s + \gamma_9 \tilde{\omega}_{\theta_{S_R}}, \tag{67}$$

$$\dot{\tilde{\theta}}_F = \gamma_{10} \tilde{v}_{x_b} + \gamma_{11} \tilde{v}_s + \gamma_{12} \tilde{\omega}_{\theta_{S_R}}. \tag{68}$$

In the system of equations (55)–(68), ϱ_k, with $k = 1 \ldots 22$, are the coefficients of the linearized dynamic equations, and γ_p, with $p = 1 \ldots 12$, are the coefficients associated with the linearized nonholonomic constraints. The analytical expressions of these coefficients have been obtained in terms of the geometric, inertial, wheels' and suspensions' parameters. Their expressions, which are overly long to be shown here, are available to the reader on request. Some comments about the linear system of equations (55)–(68) are included below.

Among the linearized equations of motion (55)–(68), Eqs. (61) and (62) are the lean and steer equations, respectively. In the works by García-Vallejo et al. [34] and Paudel et al. [35], the linearized lean and steer equations of the e-scooter were obtained by particularizing the linear equations of the bicycle benchmark by Meijaard et al. [5] for the parameters of different e-scooters designs. The lean and steer equations derived by Meijaard et al. [5] are given by:

$$\boldsymbol{M}_1 \ddot{\boldsymbol{q}} + v \boldsymbol{C}_1 \dot{\boldsymbol{q}} + \left(g \boldsymbol{K}_0 + v^2 \boldsymbol{K}_2\right) \boldsymbol{q} = \boldsymbol{f}, \tag{69}$$

where $\boldsymbol{q} = \begin{pmatrix} \phi & \delta \end{pmatrix}^\mathrm{T}$ is the generalized coordinates vector, including the lean and steering angles; $\boldsymbol{M}_1$ is the inertia matrix; $\boldsymbol{C}_1$ is the velocity dependent 'damping' matrix; $\boldsymbol{K}_0$ is the gravitational stiffness matrix; and $\boldsymbol{K}_2$ includes the gyroscopic and centrifugal effects. Lastly, $\boldsymbol{f}$ is the generalized torque vector, including the lean disturbance torque T_ϕ and the steering

torque T_δ, with $\boldsymbol{f} = \begin{pmatrix} T_\phi & T_\delta \end{pmatrix}^{\mathrm{T}}$. For $\boldsymbol{f} = \boldsymbol{0}$, Eq. (69) can alternatively be written as:

$$\ddot{\tilde{\phi}} = \beta_1 \tilde{\phi} + (\beta_2 + \beta_3 \, v^2) \, \tilde{\delta} + \beta_4 \, v \dot{\tilde{\phi}} + \beta_5 \, v \dot{\tilde{\delta}}, \tag{70}$$

$$\ddot{\tilde{\delta}} = \beta_6 \tilde{\phi} + (\beta_7 + \beta_8 \, v^2) \, \tilde{\delta} + \beta_9 \, v \dot{\tilde{\phi}} + \beta_{10} \, v \dot{\tilde{\delta}}. \tag{71}$$

The structure of the lean and steer equations (61) and (62) obtained in the present work is the same as that of the benchmark equations (70) and (71) by Meijaard et al. [5]. In particular, the coefficients ϱ_k, particularized for the hoop-shaped wheels case ($\mu_i = \sigma_i = 0$), the rigid case ($k_r \to \infty$, $k_f \to \infty$) and the undamped scenario ($d_r = d_f = 0$), are the same as the coefficients β_s, with $s = 1 \ldots 10$, of Eqs. (70) and (71). Nevertheless, the linearized lean and steer equations (69) of the bicycle benchmark by Meijaard et al. [5] are computed in a different way from the linearized equations (61) and (62). The linearized equations by Meijaard et al. [5] involve ad hoc linearization instead of systematic linearization of the nonlinear equations of motion and are derived based on Papadopoulos [42] using angular momentum balance about various axes. Furthermore, only the linearized equations associated with the lateral dynamics of the bicycle are obtained by Meijaard et al. [5]. In contrast, the linearized equations (55)–(68) derived in this work are obtained from the linearization of the nonlinear equations of motion (27)–(29). Using the linearization approach of Ref. [43], the analytical expressions of the linearized equations are obtained not only as a function of the geometric and dynamic parameters of the benchmark by Meijaard et al. [5] but also as a function of the toroidal wheels' and suspensions' parameters of the e-scooter.

In the work by García-Vallejo et al. [34], the equation associated with the forward motion is $\dot{v}_{x_b} = 0$, being decoupled from the remaining equations. Nevertheless, in the present work, the addition of the rear and front suspensions (and subsequently the coordinates θ_{S_R} and s) leads to Eq. (60), where it can be seen that the forward motion is coupled with the suspensions coordinates and their velocities. This coupling found in the model with suspensions is associated with the squat, representing the effect of the inertia on the suspensions.

4 Results and discussion

In this section, a detailed linear stability analysis is performed by resorting to the linearized equations of motion (55)–(68). The evolution of the eigenvalues with the forward speed is studied for different scenarios of interest. The chart of Fig. 8 summarizes the scenarios considered in the linear stability analysis of the e-scooter.
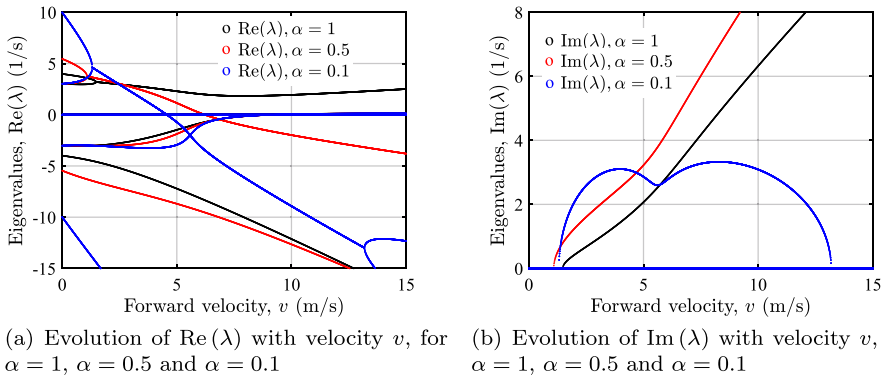
Validation of the e-scooter multibody model presented in this work First, the model of the present work is validated with the results presented by García-Vallejo et al. [34]. As previously mentioned, Eqs. (61) and (62), derived by linearizing the fully nonlinear equations of motion, yield the linearized equations by Meijaard et al. [5], used in Ref. [34], when particularized for the hoop-shaped wheels case ($\mu_i = \sigma_i = 0$), the rigid case ($k_r \to \infty$, $k_f \to \infty$) and the undamped scenario ($d_r = d_f = 0$). Obtaining the same results allows for validating the multibody model presented in this work and the linearization performed, given that the linear equations by Meijaard et al. [5] are computed using an ad hoc approach instead of linearizing the nonlinear equations of motion. The evolution of the eigenvalues with the forward speed is shown in Fig. 9 (b) and corresponds to the same linear stability results of the e-scooter benchmark presented by García-Vallejo et al. [34]
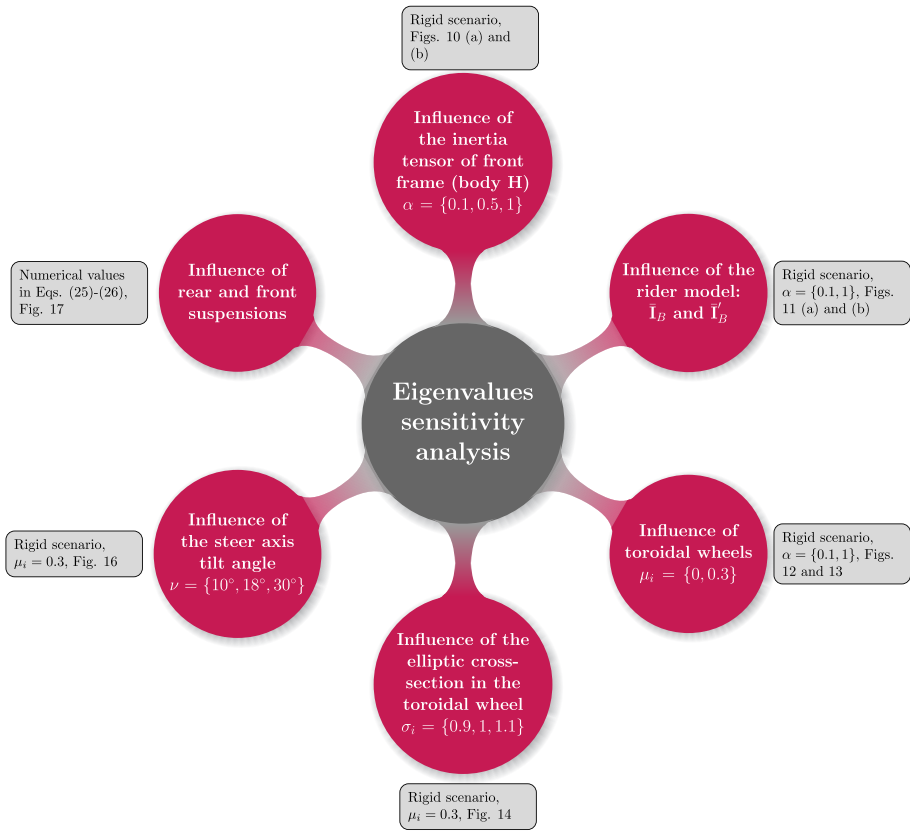
Fig. 8 Linear stability analysis of the e-scooter: eigenvalues sensitivity analysis

(a) Bicycle benchmark [5, 43]: evolution of the eigenvalues with velocity v

(b) E-scooter benchmark [34]: evolution of the eigenvalues with velocity v
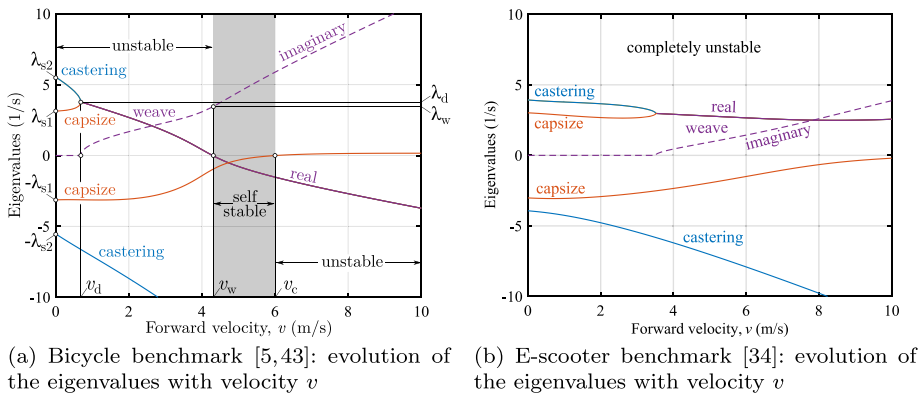
Fig. 9 Eigenvalues from the linearized speed analysis for the bicycle and e-scooter benchmarks. In contrast to the bicycle, no self-stability velocity range exists for riding the e-scooter with hands-off

(a) Evolution of $\mathrm{Re}(\lambda)$ with velocity v, for $\alpha = 1$, $\alpha = 0.5$ and $\alpha = 0.1$

(b) Evolution of $\mathrm{Im}(\lambda)$ with velocity v, for $\alpha = 1$, $\alpha = 0.5$ and $\alpha = 0.1$

Fig. 10 Influence of the moments of inertia of the front frame (body H): evolution of the real and imaginary parts of the eigenvalues from the linearized speed analysis, varying the inertia tensor of the front handlebar. The scenarios with $\alpha = 1$, $\alpha = 0.5$, and $\alpha = 0.1$ are considered

As shown in Fig. 9 (a), the uncontrolled bicycle presents a self-stability velocity range, given by $v_w < v < v_c$. The lower bound v_w is the weave speed, corresponding to the stabilization of the weave mode, and the upper bound is the capsize speed v_c for which the uncontrolled bicycle becomes unstable. In contrast, Fig. 9 (b) shows that for the numerical values of the SEAT eXS Kickscooter ES2 (see Table 1 of Appendix A), the e-scooter is completely unstable when ridden with hands-off.
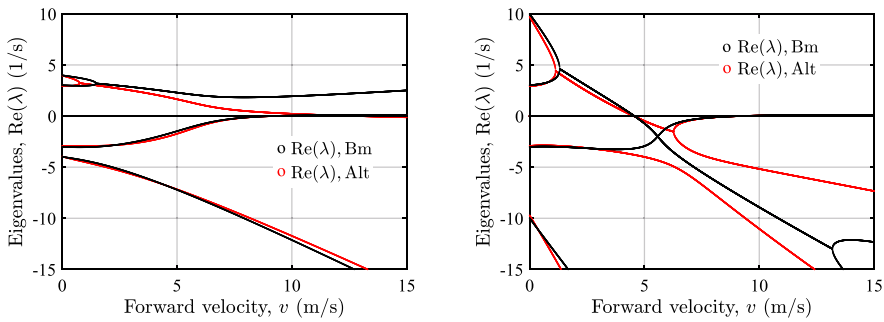
Influence of the inertia tensor of the front frame First, the influence of the inertia tensor of the front frame (body H) on the stability is studied. To this end, the evolution of the eigenvalues with the forward velocity v is computed for different moments of inertia of body H. Taking as reference the inertia tensor $\bar{\boldsymbol{I}}_H$ shown in Table 1 of Appendix A, which corresponds to the SEAT eXS Kickscooter ES2, the modified inertia tensor of body H, denoted by $\bar{\boldsymbol{I}}'_H$, is given by:

$$\bar{\boldsymbol{I}}'_H = \alpha \bar{\boldsymbol{I}}_H, \tag{72}$$

where α is a constant that allows for modifying $\bar{\boldsymbol{I}}'_H$. In this case, the mass of body H is assumed to be redistributed in such a way that the position of the centre of mass G_H is not modified.

The variation of the moments of inertia of the front frame greatly impacts on the stability of the e-scooter. These variations could arise, for instance, from modifying the location of the e-scooter battery, removing it from the handlebar. Figures 10 (a) and (b) show the evolution of the real and imaginary parts of the eigenvalues with the forward velocity, for the scenarios of $\alpha = 1$, $\alpha = 0.5$ and $\alpha = 0.1$. Despite for $\alpha = 1$ the e-scooter is completely unstable, Fig. 10 (a) shows that a decrease in α leads to the appearance of a self-stability velocity range. In particular, for $\alpha = 0.5$, the self-stability velocity range is given by $6.22 < v < 9.18$ m/s, and for $\alpha = 0.1$, this range broadens to $4.56 < v < 9.18$ m/s.

Influence of the rider model (inertia tensor of body B) As described in Sect. 2.1, the body B of the multibody model is comprised of the e-scooter deck and the rider. Due to the reduced mass of the e-scooter compared to the rider's mass, its modeling is of essential importance.

(a) Evolution of $\text{Re}(\lambda)$ with velocity v, for different inertia tensors of body B and $\alpha = 1$

(b) Evolution of $\text{Re}(\lambda)$ with velocity v, for different inertia tensors of body B and $\alpha = 0.1$

Fig. 11 Influence of the moments of inertia of body B: evolution of the real parts of the eigenvalues with the forward speed, considering the rider model in Table 1 (Bm) and an alternative inertia tensor of body B presented by Paudel et al. [35] (Alt)

A single e-scooter design presents varying performance depending on the rider's anthropometric characteristics or their riding style.

To illustrate the rider's influence on stability, the evolution of the eigenvalues with the forward speed is computed for the rider model considered in the e-scooter benchmark by García-Vallejo et al. [34] and in this study, as depicted in the CAD model shown in Fig. 3 (b) and with the inertia tensor $\bar{\boldsymbol{I}}_B$ presented in Table 1 of Appendix A. This model is referred to as 'Bm' in Figs. 11 (a) and (b). Additionally, the eigenvalues are computed for an alternative rider model with standing posture, provided by Paudel et al. [35], which is designated as 'Alt' in Figs. 11 (a) and (b). The inertia tensor of the body B considered by Paudel et al. [35], denoted by $\bar{\boldsymbol{I}}'_B$, is given by:

$$\bar{\boldsymbol{I}}'_B = \begin{pmatrix} 19.21 & 0 & -0.037 \\ 0 & \bar{I}'_{B_{yy}} & 0 \\ -0.037 & 0 & 1.78 \end{pmatrix} \text{kg m}^2. \tag{73}$$

Note that the moment of inertia $\bar{I}'_{B_{yy}}$ in Eq. (73) is not provided in Ref. [35], as it has no influence on the lateral balancing of the e-scooter.

Figure 11 shows the evolution of the real part of the eigenvalues with the forward velocity, considering both rider models. Two scenarios are studied: Fig. 11 (a) considers the inertia tensor of the front frame shown in Table 1 ($\alpha = 1$), and Fig. 11 (b) depicts the case of $\alpha = 0.1$. In Fig. 11 (a), it can be seen that the e-scooter is completely unstable for both riders' models. In contrast, Fig. 11 (b) shows a self-stability velocity range for both inertia tensors of body B. For the rider model considered in this study, the e-scooter is found to be stable for $4.56 < v < 9.18$ m/s, and for the inertia tensor by Paudel et al. [35], $4.53 < v < 9.18$ m/s. It is important to note that the evolution of the eigenvalues in Fig. 11 (b), for the scenario 'Alt', is qualitatively the same as that shown by Paudel et al. [35].

Influence of the toroidal wheels The influence of the wheels' parameters on the stability of the e-scooter is analyzed. The toroidal geometry of the wheels is considered by means of nonzero values of the tori aspect ratios μ_i. Figures 12 (a) and (b) show the evolution of the real and imaginary parts of the eigenvalues with the forward speed in the hoop-shaped and
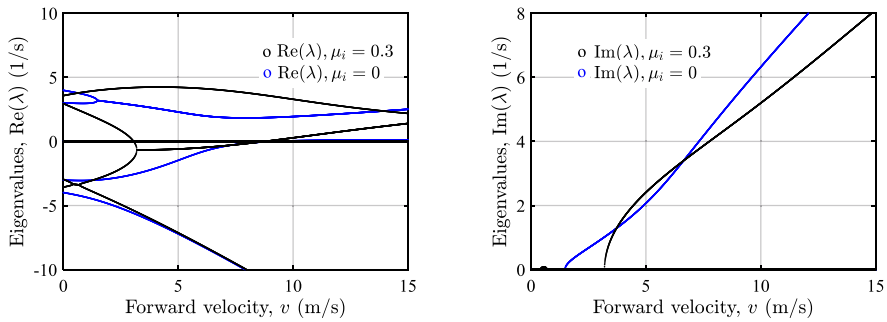
(a) Evolution of $\mathrm{Re}\left(\lambda\right)$ with velocity v: comparison of the hoop-shaped case with the toroidal wheels scenario

(b) Evolution of $\mathrm{Im}\left(\lambda\right)$ with velocity v: comparison of the hoop-shaped case with the toroidal wheels scenario

Fig. 12 Influence of the tori aspect ratios μ_i: comparison of the evolution of the eigenvalues with forward velocity, in the hoop-shaped and torus-shaped scenarios
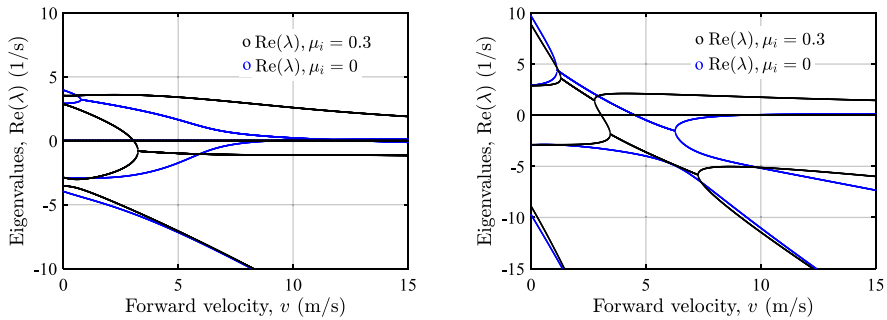
(a) Evolution of $\mathrm{Re}\left(\lambda\right)$ with velocity v: comparison of the hoop-shaped case with the toroidal wheels scenario, considering the rider inertia tensor of Paudel et al. [35] and $\alpha = 1$

(b) Evolution of $\mathrm{Re}\left(\lambda\right)$ with velocity v: comparison of the hoop-shaped case with the toroidal wheels scenario, considering the rider inertia tensor of Paudel et al. [35] and $\alpha = 0.1$

**Fig. 13** Influence of the tori aspect ratios μ_i: comparison of the evolution of the eigenvalues with forward velocity, in the hoop-shaped and torus-shaped scenarios, considering the inertia tensor of body B presented by Paudel et al. [35]

torus-shaped scenarios, respectively. The results in Fig. 12 are obtained for the numerical values of the e-scooter parameters in Table 1.

In particular, the linearized speed analysis is performed for $\mu_R = \mu_F = 0.3$, which constitute realistic values of e-scooter wheels. As shown in Fig. 12 (a), the toroidal geometry greatly impacts on the evolution of the eigenvalues, and the results vary considerably with respect to the hoop-shaped scenario. Nevertheless, despite the toroidal wheels, it can be seen that the e-scooter remains completely unstable in all the velocity range.

Figure 13 (a) shows a comparison between the hoop and toroidal wheel scenarios, when the inertia tensor of body B is considered by Paudel et al. [35]. Similar results as those of Fig. 12 (a) are obtained, with the e-scooter being completely unstable. Lastly, Fig. 12 (b) shows that the self-stability velocity range found in Fig. 11 (b), when a value of $\alpha = 0.1$ was considered, vanishes due to the destabilizing effect of the toroidal wheels.
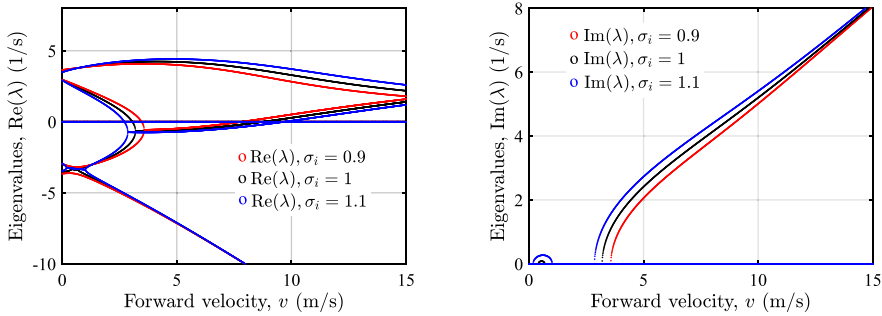
(a) Evolution of $\mathrm{Re}(\lambda)$ with velocity v: influence of the elliptic cross section, for $\mu_i = 0.3$

(b) Evolution of $\mathrm{Im}(\lambda)$ with velocity v: influence of the elliptic cross section, for $\mu_i = 0.3$

Fig. 14 Influence of the ellipses' aspect ratios σ_i: comparison of the evolution of the eigenvalues with forward velocity, for $\sigma_i = 1$ (circular cross-section), $\sigma_i = 0.9$ and $\sigma_i = 1.1$

Influence of the elliptic cross-section in the toroidal wheel The results presented so far correspond to the case of a toroidal wheel with circular cross-section ($\sigma_i = 1$). An elliptic profile of the wheel cross-section can be considered with $\sigma_i \neq 1$. Figures 14 (a) and (b) show the evolution of the real and imaginary parts, respectively, of the eigenvalues with the forward speed. The scenarios of $\sigma_i = 0.9$ and $\sigma_i = 1.1$ are compared with the circular-cross section case ($\sigma_i = 1$). It can be seen that the inclusion of the elliptic profile leads to variations in the evolution of the eigenvalues, with a lower value of σ resulting in a stabilizing effect. Note that, in any case, the e-scooter multibody model is unstable, existing eigenvalues with positive real parts.

Influence of the steer axis tilt angle The influence of the steer axis tilt angle ν on the stability is studied. As shown in Fig. 15 and described in Appendix A, the trail c, the position of the centre of mass G_H and the magnitudes x_1, b and l are a function of the angle ν. Figure 15 shows, for an arbitrary steering axis angle ν, the variation of these magnitudes with respect to the reference values shown in Table 1 (corresponding to $\nu^* = 18°$ and represented with the superscript $*$).

Figures 16 (a) and (b) show, for the hoop-shaped and toroidal wheel scenarios, respectively, the evolution of the real part of the eigenvalues with the forward speed for three different steering axis inclination angles: $\nu^* = 18°$ (reference value), $\nu = 16°$ and $\nu = 20°$. Note that an increase in ν results in a reduction of the real parts of the eigenvalues. Nevertheless, it can be seen that for the numerical values of the e-scooter parameters presented in Table 1, the variation of the steering axis angle ν does not lead to any self-stability velocity range; eigenvalues with positive real parts exist in all cases.

Influence of the rear and front suspensions So far, the results shown correspond to the rigid case. The results of the multibody model considering rear and front suspensions are now compared with the rigid scenario. In this case, the numerical values of the rear and front stiffness constants, obtained with the quasi-static tests and provided in Eqs. (25) and (26), are used instead of $k_r \to \infty$ and $k_f \to \infty$. Similarly, the null values of the rear and front damping coefficients in the undamped case, $d_r = d_f = 0$, are substituted by the numerical values obtained with the dynamic tests and presented in Eqs. (25) and (26). In the rigid case, the masses of the rear and front suspensions (m_{S_R} and m_{S_F}) are set to be null, and the
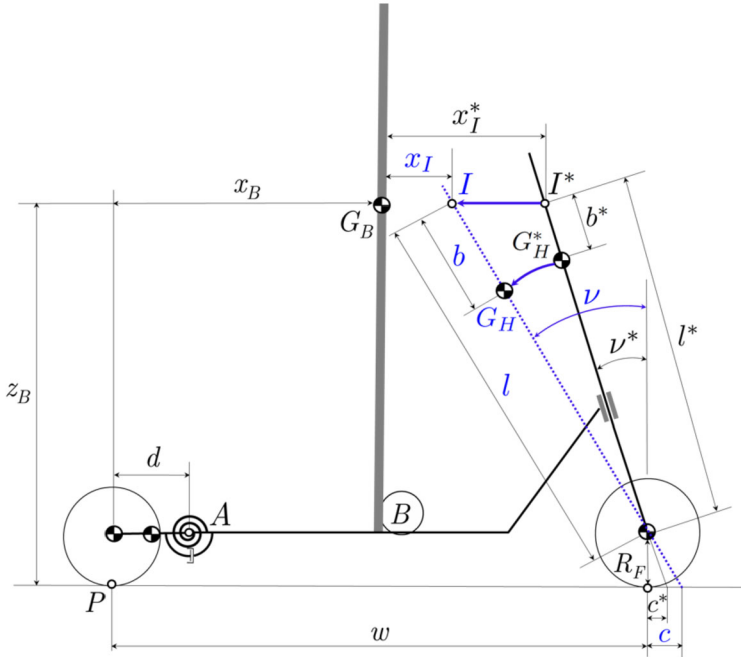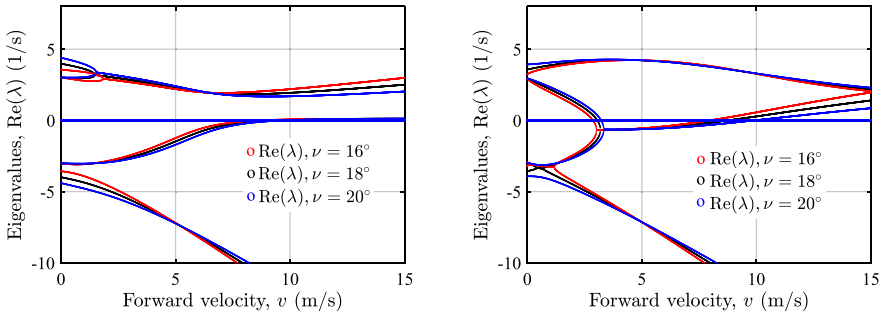
Fig. 15 Variation of the parameters c, x_I, b, l and position of G_H with the steer axis tilt angle ν


(a) Evolution of Re (λ) with velocity v: influence of the steering axis angle ν in the hoop-shaped wheels scenario

(b) Evolution of Re (λ) with velocity v: influence of the steering axis angle ν in the toroidal wheels scenario

Fig. 16 Influence of the steering axis tilt angle ν on the stability

numerical values of m_B and m_H are those found in Table 1 ($m_B = 77.5$ kg and $m_H = 8$ kg). In contrast, in the scenario considering the suspensions, $m_{S_R} = m_{S_F} = 0.5$ kg and the masses of bodies B and H are reduced, with $m_B = 77$ kg and $m_H = 7.5$ kg. Therefore, the total mass of the e-scooter is the same in both scenarios. Furthermore, given the low influence of the inertia tensors of bodies S_R and S_F on the stability, $\bar{\boldsymbol{I}}_{S_R}$ and $\bar{\boldsymbol{I}}_{S_F}$ can be assumed to be negligible (see Table 1).

Figures 17 (a) and (b) show the evolution of the real part of the eigenvalues of the e-scooter with hoop-shaped and toroidal wheels, respectively, considering the suspensions
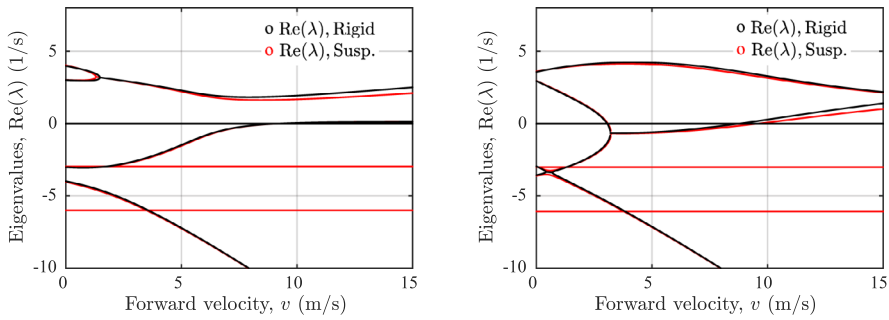
(a) Evolution of Re (λ) with velocity v: comparison of the e-scooter multibody model with rear and front suspensions with the rigid case, in the hoops-shaped wheels scenario

(b) Evolution of Re (λ) with velocity v: comparison of the e-scooter multibody model with rear and front suspensions with the rigid case, in the toroidal wheels scenario

Fig. 17 Linearized speed analysis of the e-scooter multibody model with rear and front suspensions: comparison with the rigid case

and the rigid case. The most important aspect to highlight due to the introduction of the suspensions is the appearance of two complex conjugate pairs of eigenvalues. The numerical values of the real parts of these pairs, which can be seen in Figs. 17 (a) and (b) in the suspensions' scenario (labeled as 'Susp'), are independent of the forward speed and are strongly dependent on the damping coefficients d_r and d_f. Moreover, the imaginary parts of these complex conjugate pairs strongly depend on the stiffness constants of the rear and front suspensions. Concerning the remaining eigenvalues, it can be seen that the rear and front suspensions, for this particular set of numerical values of k_r, k_f, d_r and d_f do not lead to major differences with respect to the rigid scenario (labeled as 'Rigid' in Figs. 17 (a) and (b)). To illustrate the result of the linearization, the Jacobian matrix that leads to the eigenvalues shown in Fig. 17 (b) is provided in Appendix C.

5 Conclusions

In this work, an e-scooter multibody model with toroidal wheels and suspensions has been proposed. The model is based on the SEAT eXS Kickscooter ES2. With respect to previous works in the literature, which compute the linearized lean and steer equations by using ad hoc linearization [34, 35], the nonlinear equations of motion were linearized in this paper. To this end, an efficient linearization approach, devoted to multibody systems with holonomic and nonholonomic constraints, allowed the reduced linearized system of equations along the steady forward motion of the e-scooter to be obtained. The linearized equations were computed analytically as a function of the geometric, dynamic, toroidal wheels' and suspensions' parameters of the e-scooter. The multibody model presented in this work was validated by comparing the linear stability results along the steady forward motion with the e-scooter benchmark results by García-Vallejo et al. [34]. The same eigenvalues from the linearized speed analysis were obtained.

In contrast to bicycles, for the numerical values of the e-scooter parameters considered in this work, the multibody model was shown to be completely unstable. The linear system of equations presented in Sect. 3.2 allowed performing a detailed linear stability analysis. First,

it was shown that the variation of the moments of inertia of the front frame (body H) led to significant changes in the stability of these vehicles. In particular, a reduction of the inertia tensor of the front frame (associated, for instance, with removal of the battery from the handlebar) gave rise to the appearance of a self-stability velocity range. Next, the influence of the rider model, considered by modifying the inertia tensor of body B, was studied. For both the rider model of the e-scooter benchmark [34] and Paudel et al. [35], no self-stability velocity range was found. The combined effect of the inertia tensor of body B found by Paudel et al. [35], together with the reduction of the inertia tensor of the front frame, led to an evolution of the eigenvalues with the forward speed qualitatively similar to that of Ref. [35]. Furthermore, the inclusion of toroidal wheels in the multibody model allowed studying their effect on the stability of the vehicle. In all the cases, the toroidal geometry resulted in no self-stability velocity range. Regarding the geometry of the cross-section of the toroidal wheel, a lower value of the ellipse aspect ratio results in a stabilizing effect. Similarly, the unstable behavior remained in spite of the modification of the steer axis tilt angle. Lastly, the introduction of the rear and front suspensions led to the emergence of two complex conjugate pairs of eigenvalues. The real parts of these eigenvalues, which were shown to be independent of the forward speed, are highly dependent on the damping coefficients of the suspensions, while the imaginary parts are highly dependent on the stiffness constants of the suspensions' springs. For the particular set of numerical values of the stiffness and damping constants, obtained from the quasi-static and dynamic tests, no remarkable changes with respect to the rigid scenario were found in the remaining eigenvalues. The electric kickscooter multibody model presented, together with the linearized equations of motion obtained in this work, enables a systematic analysis of the stability of these vehicles, which helps in designing new e-scooters with improved vehicle safety conditions and oriented to a wider range of potential users.

In future work, the stability analysis could be extended to more complex trajectories, such as periodic ones. Moreover, a key aspect that could be improved is the rider model, considering different postures and riding styles, the relative motion of the upper body with respect to the board, and the effect of the body support via the arms and hands on the handlebar. Lastly, the influence of different tire models on stability could also be studied.

Appendix A: List of the e-scooter multibody model parameters

The list of parameters of the e-scooter multibody model is shown in Table 1. These parameters are classified into geometric, dynamic, wheels' and suspensions' parameters.

Table 1 List of the e-scooter multibody model parameters and numerical values

	Symbol	Numerical value
Geometric parameters		
Wheel base	w	0.925 m
Trail (ref. value)	c	0.034 m
Steer axis tilt (ref. value)	ν	$\pi/10$ rad (18°)
Distance A, G_R	d	0.15 m
Distance G_{S_F}, G_F	e	0.1 m

Table 1 (*Continued*)

	Symbol	Numerical value
Dynamic parameters		
Position of centre of mass G_B	(x_B, z_B)	$(0.406, 0.912)$ m
Rider's mass	m_h	75 kg
Deck mass	m_d	2.5 kg
Mass of body B (includes the masses of the deck m_d and rider m_h)	$m_B = m_d + m_h$	77.5 kg
Inertia tensor body B	$\bar{\boldsymbol{I}}_B = \begin{pmatrix} \bar{I}_{B_{xx}} & 0 & \bar{I}_{B_{xz}} \\ 0 & \bar{I}_{B_{yy}} & 0 \\ \bar{I}_{B_{xz}} & 0 & \bar{I}_{B_{zz}} \end{pmatrix}$	$\begin{pmatrix} 13.54 & 0 & -0.22 \\ 0 & 13.39 & 0 \\ -0.22 & 0 & 1.03 \end{pmatrix}$ kg m^2
Position of centre of mass G_H (ref. values)	(x_H, z_H)	$(0.733, 0.696)$ m
Mass of body H	m_H	8 kg
Inertia tensor body H	$\bar{\boldsymbol{I}}_H = \begin{pmatrix} \bar{I}_{H_{xx}} & 0 & \bar{I}_{H_{xz}} \\ 0 & \bar{I}_{H_{yy}} & 0 \\ \bar{I}_{H_{xz}} & 0 & \bar{I}_{H_{zz}} \end{pmatrix}$	$\begin{pmatrix} 0.42 & 0 & -0.3 \\ 0 & 0.63 & 0 \\ -0.3 & 0 & 0.23 \end{pmatrix}$ kg m^2
Mass of body R	m_R	0.65 kg
Inertia tensor body R	$\bar{\boldsymbol{I}}_R = \begin{pmatrix} \bar{I}_{R_{xx}} & 0 & 0 \\ 0 & \bar{I}_{R_{yy}} & 0 \\ 0 & 0 & \bar{I}_{R_{xx}} \end{pmatrix}$	Eq. (9) and Eq. (10)
Mass of body F	m_F	1.5 kg
Inertia tensor body F	$\bar{\boldsymbol{I}}_F = \begin{pmatrix} \bar{I}_{F_{xx}} & 0 & 0 \\ 0 & \bar{I}_{F_{yy}} & 0 \\ 0 & 0 & \bar{I}_{F_{xx}} \end{pmatrix}$	Eq. (9) and Eq. (10)
Mass of body S_R	m_R	0.5 kg
Inertia tensor body S_R	$\bar{\boldsymbol{I}}_{S_R}$	$\simeq \boldsymbol{0}$ kg m^2
Mass of body S_F	m_F	0.5 kg
Inertia tensor body S_F	$\bar{\boldsymbol{I}}_{S_F}$	$\simeq \boldsymbol{0}$ kg m^2
Wheels' parameters		
Rear wheel radius	R_R	0.096 m
Rear torus aspect ratio	μ_R	Variable
Rear ellipse cross section aspect ratio	σ_R	Variable
Front wheel radius	R_F	0.105 m
Front torus aspect ratio	μ_F	Variable
Front ellipse cross section aspect ratio	σ_F	Variable
Suspensions' parameters		
Rear suspension stiffness	k_r	1202.18 Nm/rad
Rear damping coefficient	d_r	12.28 Nm/(rad/s)
Front suspension stiffness	k_f	122.05 N/mm
Front damping coefficient	d_f	221.61 N s/m

The expressions to obtain the trail c, the dimensions x_I, x_H, z_H, b and l, as a function of an arbitrary steer axis angle v and other parameters of Table 1, are shown below:

$$c(v) = R_F \tan(v), \tag{74}$$

$$x_I(v) = w + c(v) - x_B - z_B \tan(v), \tag{75}$$

$$x_H(v) = w - (l^* - b^*) \sin(v), \tag{76}$$

$$z_H(v) = R_f + (l^* - b^*) \cos(v), \tag{77}$$

$$b(v) = \frac{1}{2\cos(v)} ((x_H(v) - w - c(v)) \sin(2v) - z_H(v) \cos(2v) + 2z_B - z_H(v)), \tag{78}$$

$$l(v) = \frac{1}{2\cos(v)} (2z_B - R_F - c(v) \sin(2v) - R_F \cos(2v)), \tag{79}$$

where b^* and l^* are obtained from Eqs. (78) and (79), particularized for the reference value $v = v^* = 18°$. As specified, the numerical values of v, c, x_H and z_H in Table 1 correspond to these reference values.

Appendix B: Functions of the equilibrium configuration

The functions f_1 and f_2 of Eqs. (37) and (38) are given by:

$$f_1 \left(\theta_0, \theta_{S_R}^0, \boldsymbol{p}\right) = R_R - d \sin\left(\theta_0 + \theta_{S_R}^0\right) + (z_B - R_R) \cos(\theta_0)$$
$$+ (d - x_B) \sin(\theta_0), \tag{80}$$

$$f_2 \left(\theta_0, \theta_{S_R}^0, \boldsymbol{p}\right) = \frac{f_1 \left(\theta_0, \theta_{S_R}^0, \boldsymbol{p}\right) - R_F + x_I \sin(\theta_0)}{\cos(v - \theta_0)} - b. \tag{81}$$

The expressions of χ_1, χ_2 and χ_3, found in Eqs. (42) and (43), are:

$$\chi_1 \left(\theta_0, \theta_{S_R}^0, s_0, \boldsymbol{p}\right) = -\left(2\left((m_B + m_R + m_{S_R}) x_I\right.\right.$$
$$+ (m_R + m_{S_R}) (x_B - d)) \cos(\theta_0)$$
$$-2 (m_R + m_{S_R}) (R_R - z_B) \sin(\theta_0)$$
$$+2 ((m_B + m_R + m_{S_R}) b + m_{S_F} e$$
$$+ (m_B + m_H + m_R + m_{S_R}) s_0) \sin(v - \theta_0)$$
$$\left.+ (2m_R + m_{S_R}) d \cos\left(\theta_0 + \theta_{S_R}^0\right)\right) g, \tag{82}$$

$$\chi_2 \left(\theta_0, \theta_{S_R}^0, s_0, \boldsymbol{p}\right) = -\left(2\left((m_F + m_H + m_{S_F}) x_I\right.\right.$$
$$+ (m_B + m_F + m_H + m_{S_F}) (x_B - d)) \cos(\theta_0)$$
$$-2 (m_B + m_F + m_H + m_{S_F}) (R_R - z_B) \sin(\theta_0)$$
$$+ (2 (m_H + m_F + m_{S_F}) b - 2m_{S_F} e$$
$$+ 2 (m_F + m_{S_F}) s_0) \sin(v - \theta_0)$$

$$+ 2 \left(m_B + m_F + m_H + m_{S_F} \right) d \cos \left(\theta_0 + \theta_{S_R}^0 \right)$$

$$+ m_{S_R} d \cos \left(\theta_0 + \theta_{S_R}^0 \right)) g, \tag{83}$$

$$\chi_3 \left(\theta_0, \theta_{S_R}^0, s_0, \boldsymbol{p} \right) = 2d \cos \left(\theta_0 + \theta_{S_R}^0 \right) + 2 \left(x_B + x_I - d \right) \cos \left(\theta_0 \right)$$

$$+ 2 \left(z_B - R_R \right) \sin \left(\theta_0 \right) + 2 \left(b + s_0 \right) \sin \left(\nu - \theta_0 \right). \tag{84}$$

The functions f_3 and f_4 of Eqs. (44) and (45) are given by:

$$f_3 \left(\theta_0, \theta_{S_R}^0, \boldsymbol{p} \right) = k_f \left(s_0 - s^* \right) - \Lambda_2^0 \cos \left(\nu - \theta_0 \right) - \left(m_F + m_{S_F} \right) g \cos \left(\nu - \theta_0 \right) = 0, \tag{85}$$

$$f_4 \left(\theta_0, \theta_{S_R}^0, \boldsymbol{p} \right) = k_r \left(\theta_{S_R}^0 - \theta_{S_R}^* \right) + \Lambda_1^0 d \cos \left(\theta_0 + \theta_{S_R}^0 \right)$$

$$+ \left(m_R + \frac{m_{S_R}}{2} \right) g d \cos \left(\theta_0 + \theta_{S_R}^0 \right) = 0, \tag{86}$$

where Λ_1^0 and Λ_2^0 can be found in Eqs. (42) and (43).

Appendix C: Example of Jacobian matrix

The Jacobian matrix that leads to the eigenvalues shown in Fig. 17 (b), which corresponds to the scenario with toroidal wheels as well as rear and front suspensions, is provided. This Jacobian matrix is particularized for the numerical values of the e-scooter multibody model parameters presented in Table 1 and is given as a function of the forward velocity v. The following numerical values for the masses m_B, m_H, m_{S_R} and m_{S_F}, and the wheels' parameters μ_R, μ_F, σ_R and σ_F, are considered:

$$m_B = 77 \text{ kg}, \qquad\qquad m_H = 7.5 \text{ kg},$$

$$m_{S_R} = 0.5 \text{ kg}, \qquad\qquad m_{S_F} = 0.5 \text{ kg},$$

$$\mu_R = \mu_F = 0.3, \qquad\qquad \sigma_R = \sigma_F = 1. \tag{87}$$

The numerical values of the coefficients of the Jacobian matrix $\boldsymbol{J}$ are provided with four decimal places due to space limitations.

$$
J = \left(\begin{array}{cccccc|cccccc}
0 & 0 & 0 & 0 & 0 & 0 & 1 & 0 & 0 & 0 & 0 & 0 \\
0 & 0 & 0 & 0 & 0 & 0 & 0 & 1 & 0 & 0 & 0 & 0 \\
0 & 0 & 0 & 0 & 0 & 0 & 0 & 0 & 1 & 0 & 0 & 0 \\
0 & 0 & 0 & 0 & 0 & 0 & 0 & 0 & 0 & 1 & 0 & 0 \\
0 & 0 & 0 & 0 & 0 & 0 & 0 & 0 & 0 & 0 & 1 & 0 \\
0 & 0 & 0 & 0 & 0 & 0 & 0 & 0 & 0 & 0 & 0 & 1 \\ \hline
9.1252 & 0.1092+0.9589v^2 & 228.1646 & 10.8462 & 0 & 0 & 0 & -0.0077v & 0.4283v & 0.4198 & -6.0215 & 0.0215 \\
13.1585 & 12.6236+0.0773v^2 & 0 & 0 & 0 & 0 & 0 & -0.4111v & -0.8651v & 0 & 0 & 0 \\
0 & 0 & 342.9771 & 5.6658 & 0 & 0 & 0 & 0 & 0 & 0 & 0.3887 & -12.1580 \\
0 & 0 & -3290.9887 & -1175.6342 & 0 & 0 & -0.9061 & 0 & 0.0143 & 0.1148 & 9.6978 & 0.6080 \\
0.4120v & 0 & 0 & 0 & 0 & 0 & 0 & 0 & 0.0356 & 0 & 0 & 0 \\
1.0275v & 0 & 10.4167 & 9.5565 & 0 & 0 & 0 & 0 & 0 & 11.9037 & 0.3887 & 1.4042
\end{array}\right). \tag{88}
$$

Declarations

Competing interests The authors declare no competing interests.

References

1. Weiss, M., Dekker, P., Moro, A., Scholz, H., Patel, M.K.: On the electrification of road transportation–a review of the environmental, economic, and social performance of electric two-wheelers. Transp. Res., Part D, Transp. Environ. **41**, 348–366 (2015)
2. Whipple, F.J.: The stability of the motion of a bicycle. Q. J. Pure Appl. Math. **30**(120), 312–321 (1899)
3. Astrom, K.J., Klein, R.E., Lennartsson, A.: Bicycle dynamics and control: adapted bicycles for education and research. IEEE Control Syst. Mag. **25**(4), 26–47 (2005)
4. Limebeer, D.J.N., Sharp, R.S.: Bicycles, motorcycles, and models. IEEE Control Syst. Mag. **26**(5), 34–61 (2006)
5. Meijaard, J.P., Papadopoulos, J.M., Ruina, A., Schwab, A.L.: Linearized dynamics equations for the balance and steer of a bicycle: a benchmark and review. Proc. R. Soc. A, Math. Phys. Eng. Sci. **463**(2084), 1955–1982 (2007)
6. Kooijman, J.D.G., Schwab, A.L., Meijaard, J.P.: Experimental validation of a model of an uncontrolled bicycle. Multibody Syst. Dyn. **19**(1–2), 115–132 (2008)
7. Basu-Mandal, P., Chatterjee, A., Papadopoulos, J.M.: Hands-free circular motions of a benchmark bicycle. Proc. R. Soc. A, Math. Phys. Eng. Sci. **463**(2084), 1983–2003 (2007)
8. Escalona, J.L., Recuero, A.M.: A bicycle model for education in multibody dynamics and real-time interactive simulation. Multibody Syst. Dyn. **27**(3), 383–402 (2012)
9. Xiong, J., Wang, N., Liu, C.: Stability analysis for the whipple bicycle dynamics. Multibody Syst. Dyn. **48**(3), 311–335 (2020)
10. García-Agúndez, A., García-Vallejo, D., Freire, E.: Linearization approaches for general multibody systems validated through stability analysis of a benchmark bicycle model. Nonlinear Dyn. **103**(1), 557–580 (2021)
11. Xiong, J., Wang, N., Liu, C.: Bicycle dynamics and its circular solution on a revolution surface. Acta Mech. Sin. **36**(1), 220–233 (2020)
12. Meijaard, J.P., Schwab, A.L.: Linearized equations for an extended bicycle model. In: III European Conference on Computational Mechanics, pp. 772–772. Springer, Berlin (2006)
13. Schwab, A.L., Meijaard, J.P., Kooijman, J.D.G.: Some recent developments in bicycle dynamics. In: Proceedings of the 12th World Congress in Mechanism and Machine Science, pp. 1–6. Citeseer (2007)
14. Sharp, R.S.: On the stability and control of the bicycle. Appl. Mech. Rev. **61**(6) (2008)
15. Moore, J.K.: Human Control of a Bicycle. University of California, Davis Davis (2012)

16. Bulsink, V.E., Doria, A., van de Belt, D., Koopman, B.: The effect of tyre and rider properties on the stability of a bicycle. Adv. Mech. Eng. **7**(12), 1687814015622596 (2015)
17. Agúndez, A.G., García-Vallejo, D., Freire, E.: Linear stability analysis of a bicycle multibody model with toroidal wheels. In: Advances in Nonlinear Dynamics, pp. 477–487. Springer, Berlin (2022)
18. Bolk, J., Corves, B.: Investigation of the driving characteristics of electric bicycles by means of multibody simulation. Multibody Syst. Dyn. 1–14 (2023)
19. Sharp, R.S.: The stability and control of motorcycles. J. Mech. Eng. Sci. **13**(5), 316–329 (1971)
20. Cooper, U.R.: The effect of aerodynamics on the performance and stability of high speed motorcycles. In: Procs. the Second AIAA Symposium on Aerodynamics of Sports and Competition Automobiles, Los Angeles, California, May 11, 1974, vol. 16 (1974)
21. Jennings, G.: A study of motorcycle suspension damping characteristics. Technical report, SAE Technical Paper, (1974)
22. Sharp, R.S.: The stability of motorcycles in acceleration and deceleration. In: Inst. Mech. Eng. Conference Proceedings on Braking of Road Vehicles, London, pp. 45–50 (1976)
23. Roe, G.E., Thorpe, T.E.: A solution of the low-speed wheel flutter instability in motorcycles. J. Mech. Eng. Sci. **18**(2), 57–65 (1976)
24. Splerings, P.T.J.: The effects of lateral front fork flexibility on the vibrational modes of straight-running single-track vehicles. Veh. Syst. Dyn. **10**(1), 21–35 (1981)
25. Nishimi, T., Aoki, A., Katayama, T.: Analysis of straight running stability of motorcycles. Technical report, SAE Technical Paper, (1985)
26. Sharp, R.S.: Vibrational modes of motorcycles and their design parameter sensitivities. In: In Institution of Mechanical Engineers Conference Publications, vol. 3, pp. 107–107. Medical Engineering Publications Ltd (1994)
27. Cossalter, V., Lot, R., Maggio, F.: The modal analysis of a motorcycle in straight running and on a curve. Meccanica **39**(1), 1–16 (2004)
28. Cossalter, V., Lot, R., Massaro, M.: The influence of frame compliance and rider mobility on the scooter stability. Veh. Syst. Dyn. **45**(4), 313–326 (2007)
29. Kostrzewska, M., Macikowski, B.: Towards Hybrid Urban Mobility: Kick Scooter as a Means of Individual Transport in the City. IOP Conference Series: Materials Science and Engineering vol. 245 (2017)
30. Unkuri, J.H., Salminen, P., Kallio, P., Kosola, S.: Kick scooter injuries in children and adolescents: minor fractures and bruise. Scan. J. Surg. **107**(4), 350–355 (2018)
31. Griffin, R., Parks, C.T., Rue, L.W. III, McGwin, G. Jr.: Comparison of severe injuries between powered and nonpowered scooters among children aged 2 to 12 in the United States. Ambul. Pediatr. **8**(6), 379–382 (2008)
32. Mebert, R.V., Klukowska-Roetzler, J., Ziegenhorn, S., Exadaktylos, A.K.: Push scooter-related injuries in adults: an underestimated threat? Two decades analysed by an emergency department in the capital of Switzerland. BMJ Open Sport Exercise Medicine **4**(1), e000428 (2018)
33. Kowalczewska, J., Szymon, R., Czesław, Ż.: E-scooters and the city–head to toe injuries. J. Med. Sci. **91**(2), e672–e672 (2022)
34. García-Vallejo, D., Schiehlen, W., García-Agúndez, A.: Dynamics, control and stability of motion of electric scooters. In: The IAVSD International Symposium on Dynamics of Vehicles on Roads and Tracks, pp. 1199–1209. Springer, Berlin (2019)
35. Milan, P., Yap, F.F.: Front steering design guidelines formulation for e-scooters considering the influence of sitting and standing riders on self-stability and safety performance. J. Automob. Eng. **235**(9), 2551–2567 (2021)
36. Klinger, F., Klinger, M., Edelmann, J., Plöchl, M.: Electric scooter dynamics–from a vehicle safety perspective. In: The IAVSD International Symposium on Dynamics of Vehicles on Roads and Tracks, pp. 1102–1112. Springer, Berlin (2022)
37. Asperti, M., Vignati, M., Braghin, F.: Modelling of the vertical dynamics of an electric kick scooter. IEEE Trans. Intell. Transp. Syst. (2021)
38. Cano-Moreno, J.D., Islán, M.E., Blaya, F., D'Amato, R., Juanes, J.A., Soriano, E.: E-scooter vibration impact on driver comfort and health. J. Vib. Eng. Technol. **9**(6), 1023–1037 (2021)
39. Garman, C.M.R., Como, S.G., Campbell, I.C., Wishart, J., O'Brien, K., McLean, S.: Micro-mobility vehicle dynamics and rider kinematics during electric scooter riding. Technical report, SAE Technical Paper, (2020)
40. Brunner, P., Löcken, A., Denk, F., Kates, R., Huber, W.: Analysis of experimental data on dynamics and behavior of e-scooter riders and applications to the impact of automated driving functions on urban road safety. In: 2020 IEEE Intelligent Vehicles Symposium (IV), pp. 219–225. IEEE (2020)
41. Dozza, M., Violin, A., Rasch, A.: A data-driven framework for the safe integration of micro-mobility into the transport system: comparing bicycles and e-scooters in field trials. J. Saf. Res. **81**, 67–77 (2022)

42. Papadopoulos, J.M.: Bicycle Steering Dynamics and Self-Stability: A Summary Report on Work in Progress. Cornell Bicycle Research Project. Cornell University, Ithaca (1987)
43. García-Agúndez, A., García-Vallejo, D., Freire, E.: Linearization approaches for general multibody systems validated through stability analysis of a benchmark bicycle model. Nonlinear Dyn. **103**(1), 557–580 (2021)
44. Agúndez, A.G., García-Vallejo, D., Freire, E., Mikkola, A.: A reduced and linearized high fidelity waveboard multibody model for stability analysis. J. Comput. Nonlinear Dyn. **17**(5), 051010 (2022)
45. Diaz, R.A., Herrera, W.J., Martinez, R.: Using symmetries and generating functions to calculate and minimize moments of inertia (2004). Preprint. arXiv:physics/0404005
46. Schiehlen, W.: Multibody system dynamics: roots and perspectives. Multibody Syst. Dyn. **1**(2), 149–188 (1997)